Rute Português Eleutério
Licenciada em Bioquímica

Translocation Mechanism of Blood-Brain Barrier by peptides derived from Dengue virus – New Drug Delivery Systems

Dissertação para obtenção do Grau de Mestre em Bioquímica

Orientador: Miguel Augusto Rico Botas Castanho, Professor Catedrático, Faculdade de Medicina da Universidade de Lisboa

Co-orientador: Vera Luísa Santos Neves, Investigadora Pós-Doutoral, Instituto de Medicina Molecular

Júri:

Presidente: Prof. Doutor Pedro António de Brito Tavares
Arguente(s): Doutor Frederico Aires da Silva
Vogal: Doutora Vera Luísa Santos Neves

FACULDADE DE CIÊNCIAS E TECNOLOGIA
UNIVERSIDADE NOVA DE LISBOA
Setembro, 2016

Rute Português Eleutério
Licenciada em Bioquímica

Translocation Mechanism of Blood-Brain Barrier by peptides derived from Dengue virus – New Drug Delivery Systems

Dissertação para obtenção do Grau de Mestre em Bioquímica

Orientador: Miguel Augusto Rico Botas Castanho, Professor Catedrático, Faculdade de Medicina da Universidade de Lisboa

Co-orientador: Vera Luísa Santos Neves, Investigadora Pós-Doutoral, Instituto de Medicina Molecular

Júri:

Presidente: Prof. Doutor Pedro António de Brito Tavares
Arguente(s): Doutor Frederico Aires da Silva
Vogal: Doutora Vera Luísa Santos Neves

Setembro, 2016

Translocation Mechanism of Blood-Brain Barrier by peptides derived from Dengue virus – New Drug Delivery Systems

AGRADECIMENTOS

O trabalho desenvolvido nesta dissertação não poderia ter sido realizado sem o apoio de muitas pessoas maravilhosas!

Gostaria de começar por agradecer ao Professor Miguel Castanho por me ter dado a oportunidade de ingressar a sua equipa de investigação e por me proporcionar todas as condições necessária para a realização deste trabalho.

Um grande agradecimento à Doutora Vera Neves, por ter orientado de perto esta dissertação, pelos conhecimentos transmitidos, por toda a ajuda, confiança e incentivo demonstrado ao longo deste ano que em muito contribuíram para ampliar a minha formação científica.

Aos elementos do grupo de investigação Miguel Castanho Lab, nomeadamente à Clara, Diana, Filipa, Iris, Liliana, Marco, Mariana, Nuno, Pietro, Salomé, Sara, Susana e Tiago, pelo acolhimento, ajuda, disponibilidade e conselhos ao longo deste trabalho.

Um especial agradecimento ao Professor Francisco Enguita (Paco), pelas produtivas conversas e discussões cientificas, por toda a sua disponibilidade e incansável ajuda no que diz respeito à purificação das proteínas, o meu muito obrigada!

Gostaria também de demonstrar a minha gratidão a todos os elementos do grupo *Bioimaging*, ao José Rino, António Temudo e Ana Nascimento, por toda a atenção, ajuda, disponibilidade e transmissão de conhecimentos relativos às técnicas de microcopia de fluorescência bem como, a celeridade para ajudar na resolução dos problemas (que não foram poucos) que iam surgindo ao longo do trabalho, o meu muito obrigado, foram sem dúvida incansáveis.

Não poderia deixar também de agradecer a todos os Professores e funcionários da Faculdade de Ciências e Tecnologia da Universidade Nova de Lisboa, que ao longo destes 5 anos fizeram parte do meu percurso académico. Pela transmissão de conhecimento, por estarem sempre disponíveis, mas acima de tudo por acreditarem, confiarem, incentivarem e oferecerem as ferramentas essenciais para os seus alunos irem mais além. Mais que uma Escola, uma Família!

E porque apesar das nossas ambições e decisões nos levarem por caminhos diferentes, há sempre o factor amizade que nos ajuda a ultrapassar todos os obstáculos. Aos meus amigos, André, Andreia, Bia, Margarida, Pedro e Susana, apesar dos poucos momentos juntos, agradeço todo o apoio e por estarem sempre presentes, mesmo quando eu não conseguia estar!

Mais que uma amiga, uma irmã! Ao longo dos anos foram muitos os momentos de diversão, mas também de trabalho, de alegrias e tristezas, de sonhos, de concretizações e conquistas e, embora a distância por vezes seja grande e passem-se dias, tu estás sempre presente em todos os momentos! Obrigada por me ensinares a levar tudo com calma, a dar o melhor de mim, mas acima de tudo a levar a vida sempre com um Smile ☺ Por tudo, obrigada Ana Sofia!

Ao Odie, meu melhor amigo, meu fiel companheiro de quatro patas, obrigada por tornares tudo tão simples e verdadeiro. Não há palavras que possam descrever esta conexão, que com um

simples olhar sabias sempre quando era necessário um carinho ou uma brincadeira e, apesar da vontade de ir brincar ou de dar um longo passeio pela praia lá ficavas junto de mim, todo o dia, tornando a escrita desta tese menos trabalhosa.

Um grande agradecimento, ao Sr. Álvaro, à D.ª Lurdes e à Susana, pelo acolhimento e por todo o apoio prestado, foram sem dúvida uma preciosa ajuda ao longo deste ano.

Ao meu namorado, Luís, por toda a força transmitida, pela paciência e companheirismo, pelo permanente apoio nos bons e maus momentos, ajudando a superar os obstáculos e dificuldades com toda a tua disponibilidade, especialmente no que diz respeito à revisão linguística.

A toda a minha família, quero agradecer todo o apoio, carinho e incentivo ao longo das várias etapas da minha vida.

Um especial agradecimento à minha mãe, o meu grande pilar, por toda a força, incentivo, conselhos, dedicação e carinho. Por estares sempre presente, especialmente nos dias de maior desespero e frustração, mas essencialmente, por me dares a oportunidade de escolher o meu caminho e segui-lo sem nunca desistir, mostrando que só com trabalho e dedicação se consegue alcançar a meta. Obrigada por acreditares sempre em mim!

A todos os que aqui não foram referidos, mas que de alguma forma fazem parte da minha vida, o meu muito obrigada!

Nota: O trabalho apresentado nesta tese faz parte do projecto, TRASDRUG (PTDC/BBBNAN/1578/2014), financiado pela Fundação para a Ciência e Tecnologia (FCT).

ABSTRACT

The delivery of therapeutic molecules to the central nervous system (CNS) is hindered by poor delivery across the blood-brain barrier (BBB). Various therapeutic approaches have been developed but current delivery methods are inefficient, damage the BBB, and often lead to immune response. Therefore, successful treatment of CNS disorders requires the discovery of effective and safer drugs that are able to get across this biological barrier. Cell-penetrating peptides (CPPs) may present an opportunity to develop a drug delivery system that enables cargo trafficking through the cellular membrane and is capable of carrying different active macromolecules into the brain. Previous studies reported peptide derived from type 2 capsid protein from the Dengue Virus (DEN2C) can be employed as a CPP for brain delivery, more specifically the sequence corresponding to the third α-helix (PepH3). PepH3 specifically interacts with anionic membranes, characteristic of brain endothelial cells (BECs). In addition, preliminary results show that the translocation mechanism is receptor-independent, possibly adsorptive-mediated transcytosis. The main purpose of this thesis was to elucidate the translocation mechanism of PepH3 through BECs. To accomplish this goal, PepH3 was conjugated to green fluorescent protein (GFP) through recombinant protein technologies. Next, GFP-H3 interaction with BECs was evaluated, with a percentage of translocation of 21.63% ± 4.81 and uptake of 0.18% ± 0.10. Furthermore, inhibitory conditions and cellular staining were applied to BECs to understand cellular trafficking of GFP-H3. It was found that the cellular uptake of GFP-H3 is energy-dependent, evidenced by a decrease in translocation (4.63% ± 0.79) when cells are incubated at 4°C. In addition, of GFP-H3 translocation through BECs is inhibited by dynasore, MβCD and EIPA, confirming that an endocytic process is involved. Together the results reveal that PepH3 might function as shuttle for brain drug delivery, by interacting with anionic BECs, followed by internalization via caveolae-dependent endocytosis. By escaping lysosomes, the peptide is exocytosed into the brain side.

Keywords: cell-penetrating peptides; blood-brain barrier; drug delivery systems; translocation mechanisms; endocytosis; dengue virus capsid protein.

RESUMO

Devido à existência da barreira hemato-encefálica (BHE), a entrega de moléculas terapêuticas no sistema nervoso central (SNC) constitui um dos grandes desafios da actualidade. Ao longo dos anos, têm sido desenvolvidas novas terapias de combate às doenças do SNC. No entanto, estas são pouco eficientes, danificam a integridade da BHE ou activam respostas imunológicas. O sucesso no tratamento destas doenças requer a descoberta de fármacos, eficazes e seguros, capazes de atravessar esta barreira biológica. Para tal, péptidos capazes de a translocar são a base para desenvolver um sistema de entrega de fármacos que permita o transporte de moléculas através da BHE e consequentemente para o cérebro. Estudos efectuados com a proteína tipo 2 da cápside do vírus da Dengue, especificamente a sequência correspondente à terceira hélice (PepH3) demonstraram que esta pode servir de modelo para potenciais péptidos translocadores. O PepH3 interage especificamente com membranas aniónicas, características das células endoteliais cerebrais (CECs). Além disso, resultados preliminares demonstraram que o mecanismo de translocação é independente de receptor. O principal objectivo desta tese foi elucidar o mecanismo pelo qual o PepH3 atravessa as CECs. Para tal, o PepH3 foi conjugado com a GFP através de técnicas de biologia molecular. De seguida, foi avaliada a interacção da GFP-H3 com as CECs, tendo-se obtido uma percentagem de translocação de 21.63% ± 4.81 e 0.18% ± 0.10 de absorção. De modo a compreender a rota celular da GFP-H3, foram efectuados estudos quer com inibidores quer através da marcação dos compartimentos celulares tendo-se verificado que a translocação da GFP-H3 é dependente de energia pois, há um decréscimo da percentagem de translocação (4.63% ± 0.79) quando as células são incubadas a 4ºC. Além disso, verificou-se também que dyansore, MβCD e EIPA, funcionam como inibidores, confirmando que a endocitose está envolvida na sua internalização. Os resultados obtidos neste trabalho, revelam que o PepH3 pode funcionar como transportador de fármacos através da BHE através da interacção com CECs seguido da internalização através de endocitose dependente de *caveolae*.

Palavras-chave: péptidos com capacidade de translocação; barreira hemato-encefálica; sistemas de libertação controlada; mecanismos de translocação; endocitose; proteína da cápside do vírus da dengue.

TABLE OF CONTENTS

FIGURE INDEX

TABLE INDEX

ABREVIATIONS

ABC	ATP binding cassette
AJ	Adherent juntions
AMT	Adsorptive-mediated transcytosis
Antp	Antennapedia homeodomain
APS	Ammonium persulfate
ATCC	American type culture collection
BBB	Blood-brain barrier
BECs	Brain endothelial cells
BLAST	Basic local alignment search tool
BSA	Bovine serum albumin
CNS	Central nervous system
CO_2	Carbon dioxide
CPP(s)	Cell-penetrating peptide(s)
CPZ	Chlorpromazine
DEN2C	Capsid of the Dengue virus
dH_2O	Ultrapure deionized water
DMEM	Dulbecco's Modified Eagle's Medium
DNA	Deoxyribonucleic acid
DTT	Dithiothreitol
E. coli	*Escherichia coli*
EIPA	5-(N-Ethyl-N-isopropyl)amiloride
FBS	Fetal bovine serum
FD40	Fluorescein iso-thiocyanate dextran, 40 kDa
FLIP	Fluorescence Loss in photobleaching
FRAP	Fluorescence recovery after photobleaching
GFP	Green fluorescent protein
HCl	Chloric acid
HEPES	4-(2-hydroxyethyl)-1-piperazineethanesulfonic acid
HIV	Human Immunodeficiency Virus

IPTG	Isopropyl β-D-1-thiogalactopyranoside
KCl	Potassium chloride
KH_2PO_4	Potassium dihydrogen phosphate
LB	Lysogeny broth
MCAC	Metal-Chelate Affinity Chromatogrphy
$MgCl_2$	Magnesium Chloride
MOPS	(3-(-N-morpholino)propanesulfonic acid
MRP	Multidrug resistant protein
MβCD	Methyl-β-cyclodextrin
Na_2PO_4	Sodium hydrogen phosphate
NaCl	Sodium chloride
NaOH	Sodium hydroxide
NLS	Nuclear localizing signal
O.D.	Optical density
PAGE	Polyacrylamide gel electrophoresis
PBS	Phosphate-buffered saline
PCR	Polymerase Chain Reaction
Pen Strep	Penicillin Streptamicyn
PepH1	α_1-helix domain peptide
PepH2	α_2-helix domain peptide
PepH3	α_3-helix domain peptide
PepH4	α_4-helix domain peptide
PepM	Membrane-binding peptide
PepR	RNA-binding peptide
PPC	Particles per cell
PTT	Penetratin
RMT	Receptor-mediated transcytosis
RNA	Ribonucleic acid
rpm	Rotations per minute
SAP	Sweet arrow peptide

SB	Super broth
SDS	Sodium dodecyl sulphate
SEM	Standard error of the mean
siRNA	Small interfering RNA
SOB	Super optimal broth
Tat	Trans-activator of transcription
TEMED	Tetramethylethylenediamine
TJ	Tight junctions
Tris	Tris(hidroximetil)-aminometano
UV	Ultraviolet

I. INTRODUCTION

I. INTRODUCTION

One the biggest challenges in biomedical sciences is the discovery of therapeutic agents that act only where needed. Many human diseases, including neurodegenerative disorders such as multiple sclerosis, Huntington's, Parkinson's and Alzheimer diseases, are presently incurable. The last one is considered the sixth leading cause of all deaths and the fifth leading cause of death in people over 65 years.[1–3] During the past decades, many new therapeutic approaches have been developed but the current methods, either invasive surgical procedures or some pharmacological methods such as chemical drugs, are associated with low transfer efficiency, damages in brain membrane integrity and often led to immune response.[2,4–6] Therefore, the biggest challenge in the treatment of central nervous system (CNS) diseases, is to discover new drugs that are safe and effective.[7]

I.1. Challenges in drug delivery: The Blood-brain Barrier

The main limiting factor to a successfully treat brain diseases is associated to the lack of effective delivery of drugs across the blood-brain barrier (BBB).[4,8,9] The BBB is the most important, selective and dynamic barrier that protects the brain against foreign organisms and unwanted substances, preventing 100% of large molecules and approximately 98% of small molecules, from accessing the brain.[10–12]

The BBB is mainly constituted by specialized **endothelial cells** that form the walls of the capillaries and represents by far the largest interface for blood-brain exchange. Followed by **basal lamina**, a matrix composed of several extracellular proteins that regulates the integrity of BBB; **astrocytes** end-feet that, cover more than 99% of the basal capillary membrane, keeping the BBB stability; and **pericytes** that regulate the BBB development and permeability (Figure I.1).[13,14]

The endothelial cells are unique, their plasma membrane divides into the apical and basolateral membrane, the first which faces the blood and the last the brain tissue. These cells are tightly connected by means of adherent junctions (AJ), which help stabilize the cell-cell interaction on the junctional zone, and tight junctions (TJ) that are composed for transmembrane proteins that effectively seal the paracellular pathway.[8,13,15]

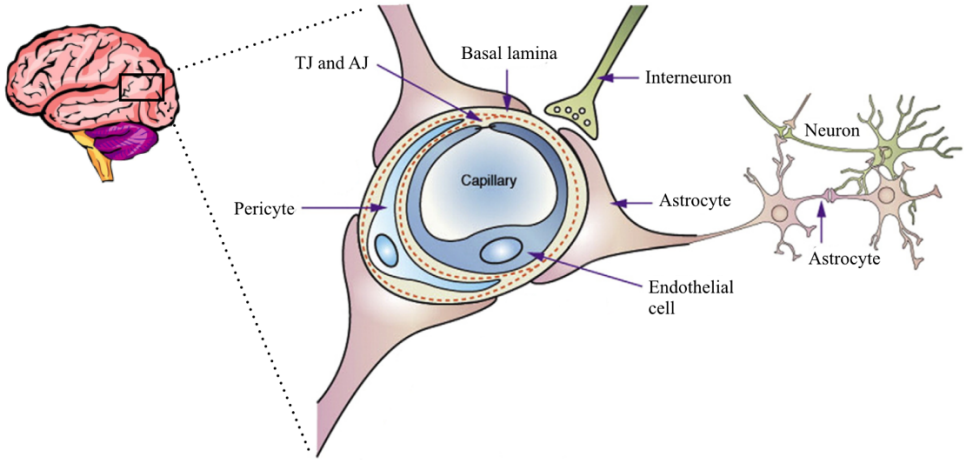

Figure I.1 - Schematic representation of the blood-brain barrier (BBB). The BBB is mainly constituted by endothelial cells that form the walls of capillaries. These cells are connected by adherent juntions (AJ) and tight junctions(TJ) and their integrity is regulated by the basal lamina, astrocytes cover the basal capillary membrane and perycites regulate the development and permeability of the BBB.[16]

Although the main function of the BBB is to protect the brain, the brain is not isolated and endothelial cells are permeable to many essential water-soluble nutrients and metabolites allowing them to be carried to the brain. Thus, several transport routes across the BBB have been identified that including two principal systems, an energy-independent direct translocation or an energy-dependent endocytosis system.[8,13,16]

Nowadays, one of the biggest obstacles in drug delivery, is to find molecules that can transport therapeutic drugs across biological membranes like the BBB. Polypeptides and oligonucleotides are generally considered to be of limited therapeutic value due to the low permeability of the BBB and to their relatively rapid degradation. Nevertheless, over the last years, it has been found that some peptides and proteins can penetrate the cell membrane and enter the cell working as safe and efficient delivery systems.

I.2. Cell-penetrating peptides: new promising therapeutic molecules

Cell-penetrating peptides (CPPs) consist of short sequences of amino acids, typically with 5-30 amino acids, that unlike most peptides are able to cross the cellular membrane and are capable of carrying different active macromolecules into cells. CPPs may thus offer new opportunities for cellular drug delivery.[17–19]

In the late 80s and early 90s, a major revolution in the identification of such transporters was recognised. The first CPPs discovered and characterized in 1988 were derived from the Human Immunodeficiency Virus (HIV), the Trans-Activator of Transcription (Tat) protein and Penetratin (PTT) protein, derived from Antennapedia homeodomain (Antp) a homeobox transcription factor of *Drosophila melanogaster*. Originally, it was discovered that the full-

length protein translocated the plasma membrane, and subsequently, mapping the domains that confer the translocation proprieties to these proteins, allowed the identification of small fragments that could efficiently enter the cells. Today, thousands of studies have been performed that aimed to characterize and optimize CPPs as cellular delivery agents leading to the discovery of many other peptides that represent a promising tool for drug delivery, particularly in neurological disorders. They can be associate to other molecules like nucleic acids, peptides or proteins as well as drugs and fluorescent or radioactive compounds for imaging, and cross the cellular membranes into the cells to deliver the intact cargo.[19–24]

I.2.1. Classes and Proprieties of Cell-penetrating peptides

CPPs constitute a very heterogeneous and large group of peptides that is often subdivided into three principal classes based on the physicochemical properties of their sequences: cationic, hydrophobic and amphipathic.[2,23]

The **cationic group**, containing approximately 83% of sequences, is considered the largest class of CPPs. Penetratin and Tat are both cationic peptides and the best-known members of this class were derived from it. In additions, cationic peptides group include homo-polymers of Arginine and Lysine. Studies based on Arginine homo-polymers (from R_3 to R_{12}), have shown that this peptide requires a minimal sequence, eight arginine residues (octaarginine, R_8), to increase the efficiency of cellular uptake. In contrast, the Poly-Lysine besides presenting the same positive net charge as arginine, has a reduced cellular uptake, because it lacks the guanidine head group. Therefore, charged residues have a crucial role in the cellular uptake of cationic CPPs because they develop electrostatic interactions with negatively charges on the cellular surface, and thus demonstrate great potential as transmembrane carriers.[2,17,23]

Amphipathic CPPs are peptides that present both hydrophilic and hydrophobic parts. These peptides can have a highly hydrophilic N-terminus and a mainly hydrophobic C-terminus. However, their "amphipathicity" is also dependent of their secondary structure, with all the polar residues pointing to one face and the nonpolar residues on the opposite side. Amphipathic CPPs group are subdivided in three sub-classes. The first sub-class comprises the chimeric peptides such as MPG and Pep-1 that were obtained by covalent attachment of a hydrophobic domain to a nuclear localizing signal (NLS) and the peptides derived from natural proteins such as pVEC, ARF (1-22) and BPrPr (1-28). The second sub-class is composed of amphipathic α-helical CPPs like MAP and transportan. These CPPs have hydrophobic and hydrophilic amino acids that occupy different faces of the helix. The third sub-class includes β-sheet amphipathic CPPs such as VT5, proline-rich amphipathic peptides such as Bac7 and sweet arrow peptide (SAP).[17,23,25,26]

The class of **hydrophobic CPPs** contains peptides from natural amino acids and chemically modified peptides. These CPPs have low global net charges because they are mainly composed of hydrophobic residues, however, they seem to be able to avoid endosomal degradation because they can cross the cell membrane directly. This class is subdivided into peptides based on natural amino acids and chemically modified ones, which include stapled peptides, prenylated peptides and pepductins.[2,17]

DNA-binding and RNA-binding proteins, heparin-binding proteins, homeoproteins, antimicrobial peptides, viral proteins and other structures, are several examples of CPPs that can be derived from natural proteins or peptides. However, is very important that the CPP are rich in basic residues, for example Argines and Lysines, that can interact with negatively charged cell surface-bound molecules.

I.3. Peptide PepH3: The peptide derived from Dengue virus

Typically, the high molecular size and charge of some proteins and other molecules as well as their toxicity or vulnerability to enzymatic degradation in the cells, are some of the difficulties peptides face to translocate the cellular membrane. So, the viral capsid proteins appear to be a great solution to solve these difficulties due to their ability to protect and deliver the viral genome into the cells. Nonetheless, employing viral capsids proteins as drug delivery systems is limited by their size.[27]

Studies reported that the type 2 capsid protein from Dengue Virus (DEN2C) has an interest sequence that can be employed as a CPP model. Dengue Viruses are members of the genus *Flavivirus* of enveloped RNA viruses and the capsid C protein is essential to ensure his specific encapsidation.[28] DEN2C is composed for 100 amino acids an occurs as a homodimer (Figure I.2). This protein interacts with both the RNA and the lipid bilayer by two peptides derived from two conserved DEN2C protein regions, one is highly cationic (RNA-binding or PepR) and the other is hydrophobic (membrane-binding or PepM). Studies with these two proteins have demonstrated that the DEN2C protein contains four α-helical regions and an intrinsically disordered N-terminal domain. PepM tends to form two highly hydrophobic α-helixes (α_2 and α_3) separated by the Pro-rich segment while PepR forms a single long α-helix (α_4), finally, studies suggest that the α_1 helix may play a role in the initial binding by rearranging the structure to further expose the hydrophobic surface (Figure I.2).[29–34]

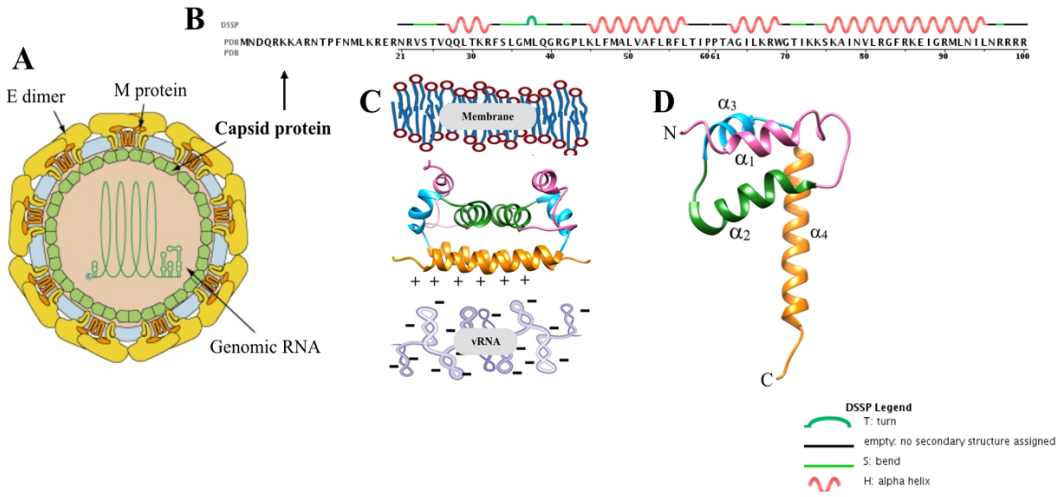

Figure I.2 - Schematic representation of Dengue Virus. **A-**Structure of genus Flavivirus virus; **B-**Amino acid sequence of DEN2C protein and it secondary structure (Protein Data Bank); **C-**Model for DEN2C molecular interactions between structural components of genus Flavivirus virus; **D-**Structure of DEN2C monomer, residues 21-100; The structures shown are based on PDB file 1R6R and were produced with Chimera v1.10.1.

Subsequent *in vitro* studies in BBB model, of these four α-helical domains showed different translocation results for each peptide. PepH2 (α_2-helix domain) presented a very low BBB translocation but a high cellular internalization while PepH4 (α_4-helix domain) had moderate membrane retention, low cellular internalization but a high BBB translocation. In the case of PepH1 (α_1-helix domain) and PepH3 (α_3-helix domain), these two peptides demonstrated a similar high potential to translocate across the BBB. However, in *in vivo* studies, where these two peptides were injected in mice only the PepH3 showed a very efficient brain uptake, a rapid excretion in high percentages and the ability to return to blood circulation. In addition, these preliminary results also show that the PepH3 translocation mechanism is receptor-independent. Possible this peptide uses an adsorptive-mediated transcytosis route, since no peptide was bound to cell membrane proteins.[35]

Although the discovery of novel efficient CPPs is progressing positively and PepH3 is a very strong candidate to translocate the BBB, the cellular uptake mechanism of this CPP continues to be an essential piece of the puzzle in the development and optimization of appropriate strategies for therapeutic applications.[36]

I.4. Cellular uptake mechanisms of cell-penetrating peptides

The BBB interposes between the systemic circulation and the brain parenchyma determining which molecules can cross it into the brain and which ones stay out. However, the brain needs essential compounds such as water-soluble molecules, glucose, essential amino acids and regulatory factors. Thus the endothelial cells enable the transport of these molecules by two

principal systems, an energy-independent direct translocation or an energy-dependent endocytosis system.[19,21,37]

The energy-independent direct translocation is a passive system where the molecules can translocate the BBB by gradient-driven route. There are two pathways, the paracellular route (Figure I.3A) translocates the small water-soluble molecules by simple diffusion through the small pores in the TJ while small lipid soluble substances dissolve in the lipid plasma membrane and are translocated across the transcellular route (Figure I.3B).[38,39]

All other molecules such as glucose, essential amino acids and regulatory factors are translocated across the BBB via an energy-dependent endocytosis system. This system can be sub-divided into five principal pathways: carrier-mediated transport; proton pump efflux transporters (efflux pumps); receptor-mediated transcytosis (RMT); adsorptive-mediated transcytosis (AMT); and cell-mediated transcytosis.[8,16,40]

Carrier-mediated transport is the pathway employed to translocate glucose and amino acids through the BBB. In this case, the molecules bind to a transporter on one side of the membrane, that through a conformational change, transports them to the other side of the membrane (Figure I.3C).[16]

The efflux pumps pathway is composed by several transporters such as ATP binding cassette (ABC) transporter, P-glycoprotein1 (P-gp) and multidrug resistant protein (MRP). These cell membrane proteins are responsible for the ejection of many foreign molecules out of cell (Figure I.3D).[8,16]

The last three systems are based on the transcytosis concept and this is the main system that macromolecules use to translocate across the BBB. Transcytosis designates the movement of cargo-packed endocytosed vesicles across the cell membrane, to a target membrane. In the membrane, the cargo is sorted in the early endosomal network where it is either recycled to the surface membrane or targeted to late endosomes and/or multivesicular bodies. Lastly, we have a fusion of cargo-packed vesicles with the target membrane and the consequent release of cargo on the other side of membrane. In RMT the macromolecules bind to specific receptors on the membrane surface and form a cluster which can translocate the membrane (Figure I.3E). The AMT systems requires cationic proteins that interact with the membrane to induce endocytosis and then the transcytosis (Figure I.3F). Finally, the cell-mediated transcytosis is a more recently identified translocation system that is mainly used by some pathogens (Figure I.3G).[8,13,16,40,41]

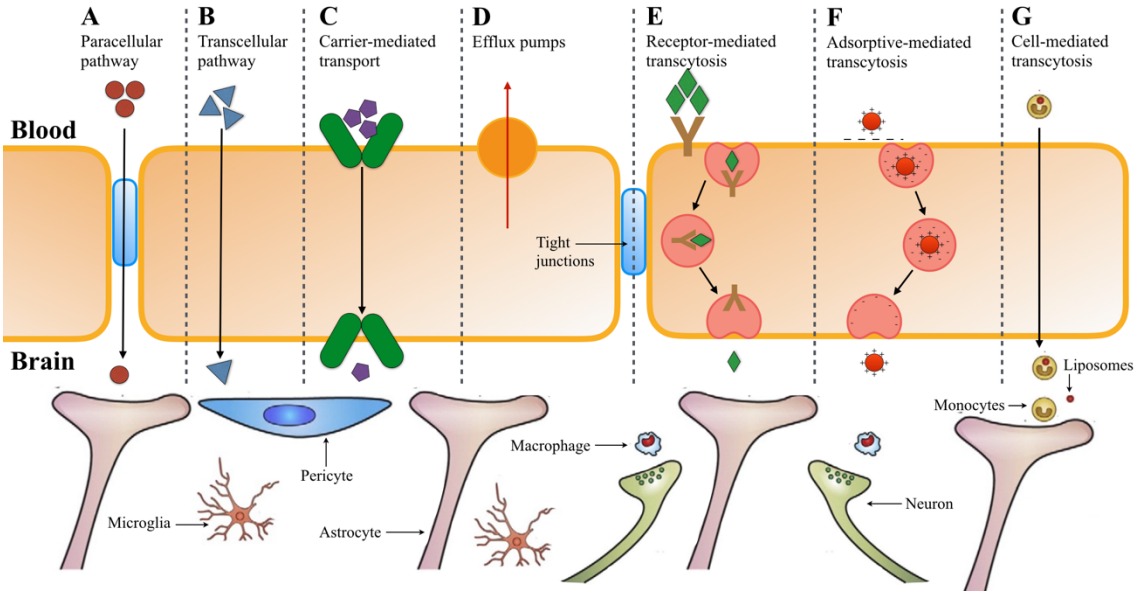

Figure I.3 - Schematic representation of the translocation mechanisms across the BBB. There are two principal systems, the energy-independent direct translocation **(A and B)** and an energy-dependent endocytosis system **(C to G)**.[16]

Several studies, employing Tat and nona-arginine, R9, have shown that these CPPs use three different endocytosis pathways belonging to the AMT systems.[42]

Internalization via an AMT mechanism is subdivided into clathrin-mediated endocytosis, caveolae-mediated endocytosis (or lipid-raft mediated endocytosis) and clathrin- and caveolin-independent endocytosis.[40,43]

Clathrin-mediated endocytosis involves the formation of clathrin-coated vesicles. The first step is the nucleation of the cargo and the binding of mediated adaptor proteins followed by the recruitment of clathrin for the clathrin coated pit. Subsequently, the large GTPase dynamin mediated twisting promotes scission and release of the vesicles. Finally, the clathrin coat is removed and the vesicles can fuse with early endosomes. From this compartment, the substances may follow a recycling route or they can suffer maturation into late endosomes that are then delivered to the other side of the membrane. Eventually the molecules can also be degraded in lysosomes (Figure I.4B).[44]

The mechanism by which caveolar vesicles (caveolae) are formed, is similar to the one described for clathrin-coated vesicles however, the caveolae are flask-shaped invaginations on cell surface. These specialized lipid-raft domains are rich in cholesterol and sphingolipids. The vesicles also recruit dynamin but, in caveolin-mediated endocytosis, the structural coat of caveolar vesicles is formed by caveolin proteins. Into the caveolae, the molecules can follow the same routes previously described or, possibly, be delivered to the Golgi apparatus or the endoplasmic reticulum (Figure I.4C).[43]

Macropinocytosis is the best identified clathrin- and caveolin-independent endocytosis mechanism and involves a cellular pathway employed when a large quantities of molecules needs to translocate the cell membrane. In this mechanism, the cell membrane forms large protrusions that are able to capture a large amount of extracellular material then, these close and form large intracellular vesicles that may undergo to various destinies. Currently, the final destination of the macropinosomes is not yet understood (Figure I.4A).[8,16,41,45–47]

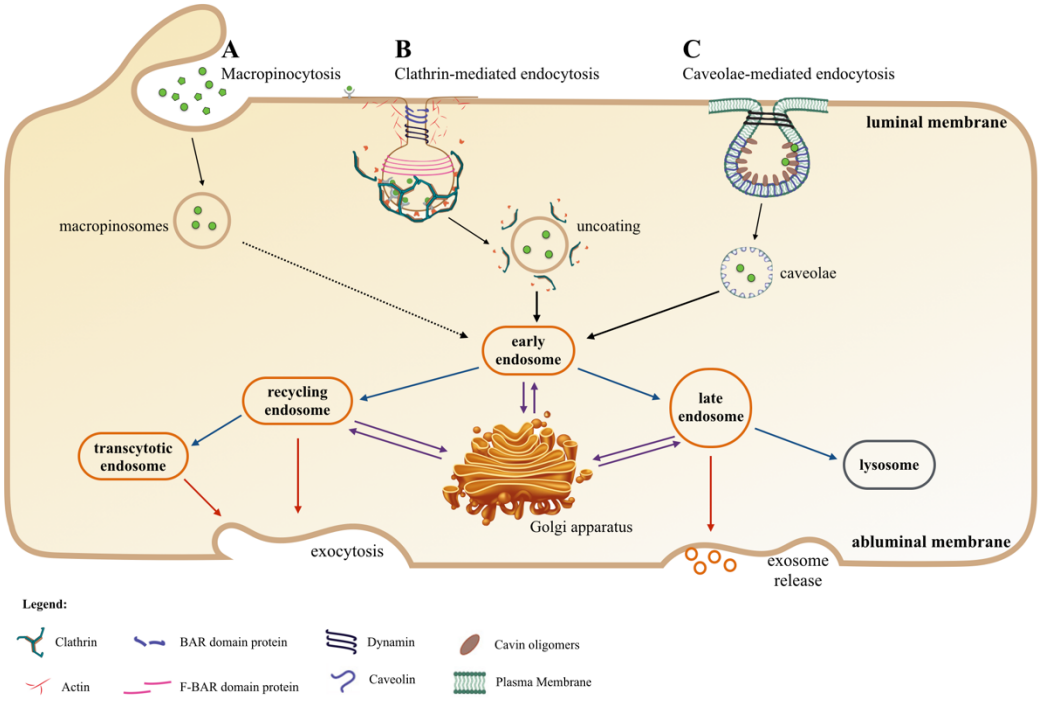

Figure I.4 - Schematic representation of the adsorptive-mediated transcytosis mechanism. There are three principal mechanisms, the macropinocytosis **(A)**, clathrin-mediated endocytosis **(B)**, and caveolae-mediated endocytosis **(C)**. The scheme was adapted from[41,48]

Although, there are several proposed mechanisms for CPP internalization and translocation of the BBB, the true mechanism employed by each CPP might be dependent on a variability of both chemical and physical factors. The CPPs characteristics such as their sequence, size, charge, structure and stability as well as the characteristics of their cargo such as its structure or charge can also contribute for their translocation.[45,49] For example, the mechanism that allows for the translocation of the Tat peptide depends on its cargo. When Tat is conjugated with a protein, it uses a lipid-raft mediated endocytosis but, when it is conjugated with a fluorophore it uses a clathrin-dependent endocytosis. The peptide concentration as well as the cell type-dependent composition of the plasma membrane also can contribute for the CPP translocation.[22,26,47]

I.5. Strategies to study the cell-penetrating peptides translocation on BBB

I.5.1. Cell models as tools to study the BBB

The pharmaceutical drug discovery and development processes are divided into different stages that culminate with the submission and launch of the final product. The discovery phase is very important because it is the phase where *in vitro* and *in vivo* studies are performed.

In the initial phase, choosing the correct models of the BBB is crucial because cell-based BBB assays are powerful and flexible experimental tools that allow us to study the transport processes and the dynamic functions of the BBB in normal and pathological states. To study the response of the BBB and determine its permeability, the *in vitro* BBB cell models are usually isolated from mouse, rat and human tissues. Outside the cost, time and cell capacity, it is very important that the model resembles the *in vivo* conditions and that other important conditions are respected, such as a reproducible permeability of reference compounds, a good screening capacity, the display of complex tight junctions, adequate expression of BBB phenotypic transporters and transcytosis activity. However, the choice of BBB cell model depends on what the objective and/or the stage at which the drug discovery experiment is at.[15]

I.5.2. Application of cell models as tools to study the trafficking pathways

One of the most important phases on drug discovery is the pharmacodynamics studies as well as the BBB permeability studies, time course and determination of free drug concentrations in blood and brain. To accomplish these studies, the brain endothelial cells are grown on filter inserts together with culture medium at the bottom of culture plates to simulate the physiologic conditions (Figure I.5).[15,50]

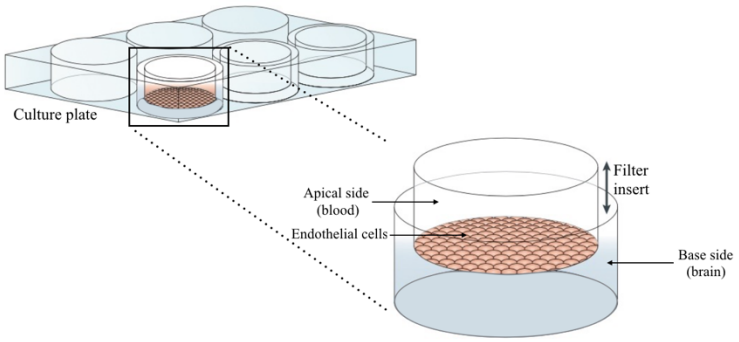

Figure I.5 - Schematic representation of the *in vitro* blood-brain barrier model. The filter inserts are placed into culture plates to simulate the different parts of the BBB. The endothelial cells are cultured into apical side where are applied the samples to simulates the blood side. The base side represent the brain side where culture medium can be added. The scheme is adapted from[15]

These modelling can be used for study the trafficking pathways by perturbation of cellular transport. Most transport processes are affected by therapeutic agents that can interfere with some specific characteristics of cell function or structure. Thus by inhibiting a specific pathway, it is possible to understand that the main structures, proteins and other cellular components which are essential and involved in CPPs translocation.[15,51]

I.5.3. Fluorescent labelling to study the trafficking pathways

As aforementioned, CPPs have a great potential as carriers of various types of cargos into cells such as peptides, proteins, including antibodies, nucleotides, siRNA, plasmids, imaging agents, drugs and other molecules.[22,52]

One the most effective strategies that allow for the study of these delivery proteins is the fusion of CPPs with fluorescent probes in order to analyse their location, translocation dynamics and to quantify them in both *in vitro* and in *in vivo* experiments, through fluorescence techniques.

The principal fluorescent probe employed in this studies is the green fluorescent protein (GFP). This protein was isolated from the pacific jellyfish *Aequorea victoria* and it revolutionised cell biological research allowing the visualization of protein dynamics inside living cells. The native GFP structure is composed by 238 amino acids making up the 27 kDa that form a 11 β-sheets that are arranged in a rigid cylindrical β-barrel structure. The significant and stable fluorescence is derived from a triplet of adjacent amino acids, seryne-tyrosine-glycine at positions 65-67 which are located in the center of a stable barrel structure (Figure I.6). The fluorescent specie is formed through a reaction that occurs between the amino acids triplet and it exists in two states, a protonated form that absorbs at 395 nm and is the prevalent state of GFP and an unprotonated one that absorbs at 475 nm. GFP has a maximum fluorescence emission peak at approximately 509 nm (Figure I.7).[53–55]

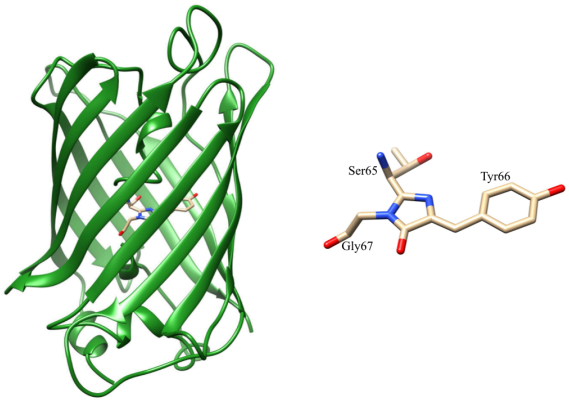

Figure I.6 - Structure of Green fluorescent protein (GFP). **Left:** Three-dimensional view of GFP β-barrel structure. **Right:** GFP chromophore is an amino acids triplet (Ser65-Tyr66-Gly67) which are located in the center of GFP β-barrel structure. The structures shown are based on PDB file 1ema and were produced with Chimera v1.10.1.

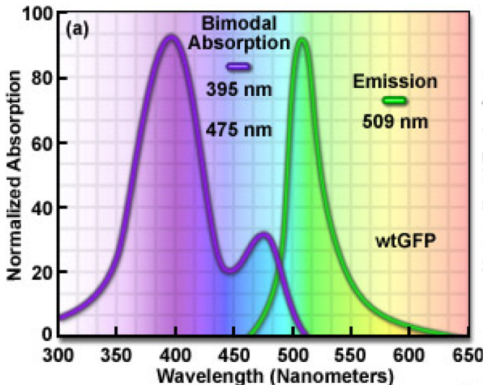

Figure I.7 - Absorption and emission spectrum of wild type green fluorescent protein (wtGFP). The spectrum shown is adapted from Zeiss.[56]

Today it is possible to find a broad variety of fluorescent protein genetic variants that have been developed to provide a wide range of fluorescence emission spectral profiles that span almost the entire visible light spectrum.[53–55]

These approaches have expanded and adapted the use of fluorescence labelling allowing it to be used in almost every biological study. In live cells, fluorescent proteins are usually employed to ascertain the localization and trafficking of proteins, organelles, and other cellular compartments.[54,57]

I.5.4. Fluorescence techniques to study the trafficking pathways

Fluorescence microscopy of living or fixed cells is an essential technique in biological and biomedical sciences to observe the dynamic processes inside the cells and tissues but for each

study it is of the utmost importance to choose the best suited system to use. Confocal Microscopy and Wide-field are the two principal modes of light microscopy.[51,58,59]

In wide-field microscopy the sample is subjected to intense illumination from a mercury or xenon arc-discharge lamp. The fluorescence emission is detected by diode array and the resulting image can be viewed directly in the ocular or captured by a CCD image sensor and viewed in a computer (Figure I.8A).[54,60–62]

Confocal microscopy consists of multiple laser excitation sources, a scan head with optical and electronic components, electronic detectors (photomultipliers) and a computer for acquisition, processing, analysis, and display of the images. The sample is excited by lasers and the scan head rasterizes the excitation scans and collects the photon signals that are required to assemble the final image. One of the most important components of the scan head is the pinhole aperture. Whereas in wide-field microscopy all of the light emitted by sample is captured, including light from outside of the focal plane, resulting in a significant amount of the signal being due to emitted background light and autofluorescense, the confocal microscope uses a pinhole that focuses a spot of light that is centered in the focal plane to eliminate out-of-focus light resulting in images of a greater clarity. In this technique the fluorescence emission signal that is passed through the pinhole aperture is converted into an analogue electrical signal by the photomultiplier that is then converted to pixels (Figure I.8B).[54,60–62]

Confocal microscopy presented numerous advantages when compared with conventional wide-field microscopy namely, the ability to control the field depth, the reduction of complete elimination of background information away from the focal plane and the capability to collect serial optical sections (z-stack) from thick samples.[54,60–62]

Presently, trafficking itineraries and cellular dynamics are increasingly being analysed through a 4D technique, meaning that the analysis is being made in the three spatial dimensions over time. Nonetheless, fluorescence recovery after photobleaching (FRAP) and fluorescence loss in photobleaching (FLIP) are other modes of microscopy that facilitate the study of diffusion of molecules whiting living cells.[51,63]

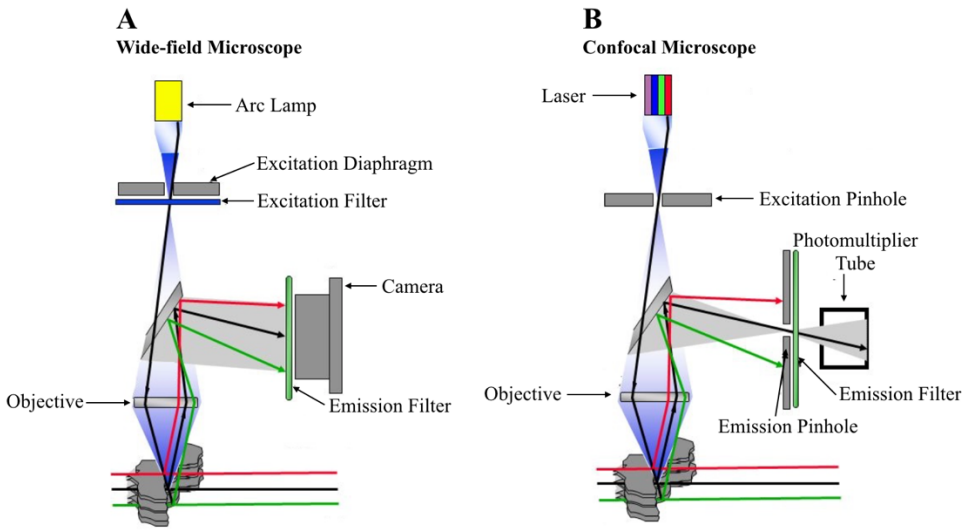

Figure I.8 - Schematic representation of the two principal modes of light microscopy. **A –** Principal components of wide-field fluorescent microscope; **B –** Principal components of Confocal microscope.

I.6. Subject and objective of this work

The need to deliver drugs into the brain to treat neurological diseases such as Alzheimer's disease has been a major challenge in recent years. However, as the brain cells need to be strongly protected against infections, toxins or other foreigner molecules that may enter the bloodstream, the BBB acts as a highly selective permeability barrier that only allows certain molecules, needed for metabolism and maintenance of these cells, to cross it, effectively separating the circulating blood from the brain tissue.

Owning the barrier properties, the challenge is not to simply create new drugs to counteract on neurological diseases, but trying finding means of bringing these drugs across the BBB into the brain where they are needed and where they can fulfil their function. The drug delivery system cannot result in lesions to the brain cells or in a change to their permeability. It is therefore necessary to develop a system that on one hand leaves the cells intact but on the other is efficient in its role of translocating the drug to the brain.

The discovery and study of cell-penetrating peptides have proven to be a good strategy to develop new drug delivery systems to the brain as these peptides can easily cross cell membranes, carrying other molecules with the added advantage of being almost free of toxic effects.

Recent studies have shown that the capsid proteins of the Dengue virus may give rise to multiple sequences that can be derived into CPPs. Nevertheless, before using an CPP as a drug delivery system it is important to understand how it operates, what is its internalization mechanisms and if there are any toxicological effects to the cells.

The main purpose of this work is to elucidate the translocation mechanism of PepH3 derived from the capsid protein of the Dengue virus. To accomplish this, the PepH3 will be conjugated with GFP using molecular biology techniques. Subsequently, the conjugate GFP-PepH3 will be cloned into expression vectors and transformed into competent cells. After expression, the conjugate will be purified in order to obtain a large amount of protein to perform cellular assays.

On the second part of this work, the GFP-PepH3 will interact with brain endothelial cells in different conditions. Thus, allowing to establish a mechanism of translocation, either through an energy-independent direct translocation or an energy-dependent endocytosis system. For a more detailed study of an energy-dependent endocytosis pathway, inhibitors of specific cellular trafficking pathways will be used. Lastly, these results will be confirmed using fluorescence microscopy techniques. Through live-cell images it will be possible to observe the effect the peptide and the inhibitors have on the cells as well as the interaction of the GFP-PepH3 in the different cellular compartments in order to understand the translocation mechanism of this peptide.

II. MATERIALS AND METHODS

II. MATERIALS AND METHODS

All reagents used throughout this work as well as their purity and brand are summarized in Appendix Table VI.11. All solutions were prepared with ultrapure deionized (dH_2O) water filtered through a PES 0.2 μm filter and autoclaved.

II.1. Recombinant Protein GFP-Pep

The oligonucleotides used in this work were designed using the Thermo Fisher Scientific tools and purchased at the same company. Forward sequence that aligns with the initial sequence of the gene contains the restriction site for restriction enzyme (NheI or NcoI) sequences whereas the reverse sequence aligns with the final sequence of the gene contains the restriction site for XhoI, linker and peptide sequences. The primers aliquots were prepared in dH_2O DNase/RNase free and stored at a concentration of 20 pmol/μL.

II.1.1. Amplification for Polymerase Chain Reaction (PCR)

The PCR mix solution used for the PCR reaction was prepared according to Table II.1for a total volume of 20 μL. For the positive control the following solutions were added: 0.5 μL of DEN2C (DNA), 0.3 μL of DEN-sfi F (Primer Forward) and 0.3 μL of DEN-sfi R (Primer Reverse) and for the negative control 0.5 μL of dH_2O DNase/RNase free were added.

Table II.1 - PCR mix solution, components and volumes.

Components	Volume (μL)
DNA	0.5
Primer Forward	0.3
Primer Reverse	0.3
Master Mix (KOD)	10
dH_2O	8.9
Total Volume	**20**

PCR amplifications were performed with PCR Thermo cycler (Biometra Tpersonal48, Analytikjena) under the following conditions:

Table II.2 - DNA PCR amplification conditions.

Step	Conditions
(1) Polymerase activation	95°C for 2 min
(2) Denaturation	95°C for 30 sec
(3)Annealing	60°C for 30 sec
(4) Extension	70°C for 30 sec
Repeat steps 2 to 4	30 cycles

Colony PCR amplifications were prepared from four colonies transformed into *Escherichia coli* (*E. coli*) dH5α competent cells (Thermo Fisher Scientific). Each colony was suspended in 20 µL of dH_2O.

Table II.3 - Components and volumes for colony PCR mix solution.

Components	Volume (µL)
DNA	4.7
Primer Forward	0.15
Primer Reverse	0.15
Master Mix	5
Total Volume	**10**

Table II.4 - Colony PCR amplification conditions.

Step	Conditions
(1) Polymerase activation	95°C for 7 min
(2) Denaturation	95°C for 30 sec
(3)Annealing	60°C for 30 sec
(4) Extension	70°C for 30 sec
Repeat steps 2 to 4	30 cycles

All amplification products were visualized under ultraviolet (UV) light (ChemiDoc™XRS+, Bio-Rad) in a 2% (w/v) electrophoresis ultrapure grade agarose gel in TBE1x buffer.

Plasmid DNA was purified with a QIAquick Gel Extraction kit (QIAGEN). Followed by DNA precipitation using a sodium acetate solution (20 µL sodium acetate, 500 µL ethanol 100% and 1 µL glycogen), samples were stored at -80°C. The precipitated DNA was ressuspent in dH_2O and all samples were quantified using NanoDrop 2000 Spectrophotometer (Thermo Fisher Scientific).

II.1.2. DNA Digestion

Amplified sequences were inserted in a pET28a (+) or pETM-10 vector containing a His-Tag in the N-terminal.

For pET28a (+) cloning, sequences were ligated into the NheI and XhoI restriction enzyme cleavage sites upstream of pET28a (+) vector. First, DNA was digested with NheI restriction enzyme. For the digestion of 1 μg of DNA, it was added 2 μL Tango buffer (10x), 0.5 μL NheI (10U, one unit required to digest 1 μg of lambda DNA) and dH_2O to make up to a total volume of 20 μL, followed by incubation overnight at 37°C. Next, the DNA was precipitated with sodium acetate, as previously described. This step is required to exchange buffer components of the digestion reaction. For the digestion with XhoI 1 μg of DNA, was added to 2 μL R buffer (10x), 0.5 μL XhoI (10U, one unit required to digest 1 μg of lambda DNA) and dH_2O to make up to a total volume of 20 μL and incubated overnight at 37°C.

Amplified sequences to be inserted in the pETM-10 vector were digested with the restricton enzymes NcoI and XhoI. In this case, the digestion of DNA occurs simultaneously. The digestion was performed using 1 μg of DNA, 4 μL Tango buffer (10x), 0.5 μL NcoI (10U), 0.5 μL XhoI (10U) and dH_2O to make up to a total volume of 20 μL and the solution was incubating overnight at 37°C.

Subsequent to the digestion procedure the DNA was purified using a PCR Clean kit (QIAGEN) and quantified using NanoDrop 2000 Spectrophotometer (Thermo Fisher Scientific).

II.1.3. Cloning and Transformation into competent cells

For cloning the amplified and digest DNA fragments (200 ng) were inserted into pET28a (+) vector in a proportion of 1:3 (200 ng of insert to 65 ng of vector), using a CloneDirect ligation kit. For ligation reaction to the respective volumes of insert DNA and vector it was added 2 μL of 10x Ligation buffer, 1 μL of CloneSmart DNA Ligase, and dH_2O to make up to a total volume of 20 μL. The reaction was incubated at 23ºC for 2 hours, and then stopped by incubating the reaction at 70ºC for 15 minutes.

Ten microliters of the plasmid solution were added to 70 μL of *E. coli* dH5α competent cells (Thermo Fisher Scientific) and incubated in SOB medium at 37ºC, 225 rpm (Incubator Orbital Shaker, VWR) for 1 hour. The transformed cells were grown overnight in LB plates with 50 μg/mL of Kanamycin. Four random colonies were picked for PCR amplification (see the procedure in II.1.1). After amplification two of the colonies were selected for sequencing at GATC Biotech.

The positive sequences were transformed in *E. coli* BL21(DE3) competent cells (Thermo Fisher Scientific) in the same conditions as those for *E. coli* dH5α competent cells.

For detailed composition and preparation of the medias, please refer to Appendix Table VI.1.

II.2. Protein Expression and Purification

Cells were grown in 500 mL SB medium (Appendix Table VI.1), supplemented with kanamycin (50 μg/mL), at 37ºC until an $OD_{600} \cong 0.6$ was reached and then induced with 0.6 mM IPTG at 25ºC, 200 rpm (Incubator Orbital Shaker, VWR) for approximately 20 hours. Cells were harvested by centrifugation (JE-21M/E Centrifuge, Beckman) at 4°C, 4000 rpm for 15 minutes. The pellet was re-suspended in 25 mL of Binding buffer with anti-proteases and stored at -20ºC. The frozen pellets were thawed at 4ºC and 5 μL of Benzonase (10 μL for 50 mL of protein extract) were added. Subsequently the cells were incubated on ice for 30 minutes and lysed by sonication on ice for 6 minutes (three 2 minute cycles of 50% pulsing). The lysate was cleared by centrifugation (Centrifuge 5418 R, Eppendorf) at 4°C, 13 000 rpm for 45 minutes.

The supernatants were purified by Metal-Chelate Affinity Chromatography (MCAC) to remove the contaminants. The protein extract was purified using a 5 mL HisTrap column (GE Healthcare Life Sciences) on an ÄKTA Explorer (GE Healthcare Life Sciences) with a flow of 1 mL/min. After injection, the protein extract was washed with Buffer A (50 mM Sodium phosphate, 1 M NaCl and 10% glycerol, pH 6.8), the proteins that not adsorbed were washed out. The protein of interest was eluted employing a discontinuous linear gradient with Buffer B (50 mM Sodium phosphate, 1 M NaCl, 500 mM Imidazole and 10% glycerol, pH 6.8) as follows: 5% for injection, 12% for washed and 12% - 100% for elution (4 volumes/column) for 20 minutes. The absorbance of the eluate was monitored at 395 nm, the first GFP absorbance pick. To ensure protein stability and further purify the protein extract a molecular exclusion chromatography was performed using HiLoad 16/60 Superdex S200 column (GE Healthcare Life Sciences) on an ÄKTA Explorer (GE Healthcare Life Sciences) with a flow of 1 mL/min. The proteins were eluted with PBS with 1mM DTT and the eluate absorbance was monitored at 280 nm and 395 nm. A flowchart of these procedures is depicted in Appendix Figure VI.3.

Protein samples were concentrated with an Amicon® Ultra-15 (Merck) at 4°C, 4000 rpm for 30 minutes. The concentrated proteins were quantified in a Nanodrop ND-1000 Spectophotometer (Thermo Fisher Scientific) by measuring the absorbance at 280 nm and employing the corresponding extinction coefficient and molecular weight (ProtParam Database). Protein quantifications were also confirmed by Bradford Method (Appendix VI.6) and protein purity was analysed by SDS-PAGE electrophoresis in 12% of acrylamide gels (Appendix VI.7). Protein samples were stored in aliquots at -80ºC in PBS with 1mM DTT and 10% of glycerol.

II.3. GFP-pep Interaction with Brain Endothelial Cells (BECs)

II.3.1. Cell Line and Cell Culture

Immortalized mouse brain endothelial cell line bEnd.3, purchased from the ATCC®, were used to simulated the blood-brain barrier. Cells were cultured in complete Dulbecco's Modified Eagle's medium (DMEM, Gibco, Thermo Fisher Scientific), supplemented with 10% fetal bovine serum (FBS, Gibco, Thermo Fisher Scientific) and 1% Penicillin Streptomycin (Pen Strep, Gibco, Thermo Fisher Scientific). Cells were grown on T-75 flasks in an incubator at 37°C with 5% CO_2 atmosphere and the medium was changed every two days.

When the adherent monolayer reached 80% confluency, cells were harvest with trypsine (Gibco, Thermo Fisher Scientific) and seeded either 3500 cell/well into tissue culture inserts (pore size 1 μm, Falcon) coated with fibronectin (Merck) in 24-well plates (Falcon); or 6000 cell/well in 24-well plates (Costar) without tissue culture inserts. The cells were grown for 9 days until tight junctions were formed and the media was changed every two days.

II.3.2. Peptide Translocation, Integrity and Internalization in BBB model

The bEnd.3 cells grown in tissue culture inserts were incubated with 0.5 μM of different peptide-conjugates (GFP, GFP-Tat, GFP-PTT and GFP-H3) in DMEM without phenol red with 10 % FBS during 5 hours at 37ºC, 5% CO_2. After incubation, the samples were collected from the apical side or apex and base of the inserts. Both apex and base were washed twice with PBS and once with complete DMEM without phenol red. Next, 25 mg/mL of Fluorescein isothiocyanate-dextran (40 000 wt, FD40, Sigma) was diluted to an absorbance of 0.1 or lower and added to the apex. The plates were incubated for 2 hours at 37ºC, 5% CO_2 to verify barrier integrity.

The cellular interaction and internalization assays were performed in 24-well plates without tissue culture inserts. The cells were incubated with 0.5 μM of different peptides (GFP, GFP-Tat, GFP-PTT and GFP-H3) in complete DMEM without phenol red during 5 hours at 37ºC, 5% CO_2. After incubation, the samples were collected. To recover the protein membrane interaction samples, the cells were washed with cold PBS followed by an acid buffer (100 mM NaCl and 50 mM Glycine, pH 2.8) and again with PBS. Volumes from different washes were combined to the same eppendorf. Next the cells were lised using RIPA buffer (50 mM Tris-HCl, 150 mM NaCl, 1% Triton X-100, pH 7.2). Lised cells were collected and soluble proteins were cleared by centrifugation (Centrifuge 5418 R, Eppendorf) at 4ºC, 13 000 rpm for 15 minutes.

All fractions were analysed by fluorescence spectroscopy in a 96-well black plate (Eppendorf) with a Plate Reader (Infinite® M200, Tecan). The fluorescence signal of samples

with GFP was obtained exciting the samples at 395 nm and recording their emission at 509 nm. As for samples with FD40 the fluorescence signal was obtained exciting the samples at 493 nm and recording their emission at 560 nm.

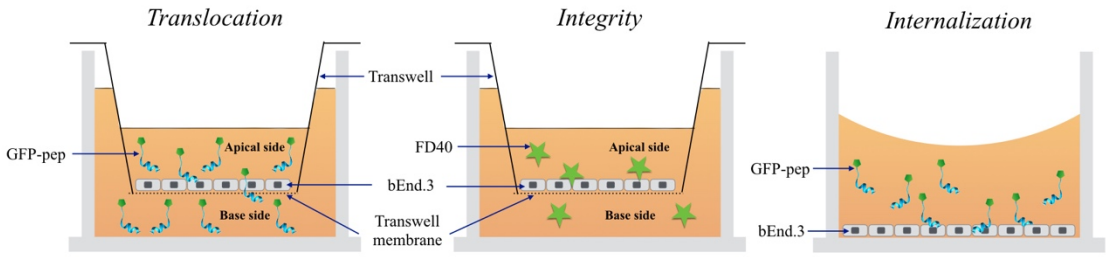

Figure II.1 - Schematic representation of BBB *in vitro* studies. First, the peptide translocation studies. In centre, the integrity tests. Lastly, the internalization and interaction studies. These studies were performed in bEnd.3 cells.

II.3.3. Metabolic and Endocytosis Inhibition Studies in BBB model

The metabolic inhibition studies were first performed at low temperature. In order to decrease the temperature gradually, the cells were maintained for 30 minutes at room temperature before adding the peptide. Cells were incubated with 0.5 µM of different peptides (GFP, GFP-Tat, GFP-PTT and GFP-H3) in complete DMEM without phenol red during 5 hours at 4ºC.

The inhibition of Clathrin-dependent and -independent endocytosis was induced by treating cells with chlorpromazine (CPZ) and dynasore, respectively, at 50 µM, 30 minutes prior to the addition of peptide. The cells were incubated with 100 µM of 5-(N-Ethyl-N-isopropyl)amiloride (EIPA) for 30 minutes to inhibited the macropinocytosis mechanism. Methyl-β-cyclodextrin (MβDC) was added at 5 mM for 30 minutes prior to the addition of peptide to block the lipid raft/caveolae-mediated endocytosis. Brefeldin A was added at 10 µg/mL for 30 minutes to interfered with the Golgi trafficking.

After peptide incubation, samples were collected from the apex and base. Next, the integrity of the BBB was evaluated for all inhibitory conditions and controls using FD40 probe, as previously described.

The fluorescence signal of all fractions was measured in a 96-well black plate with a Plate Reader (Infinite M200, Tecan) using the same parameters for GFP and FD40 samples.

II.4. Cellular pathway of peptide transmigration – Microscopy Studies

II.4.1. Confocal Microscopy – Live-Cell Imaging

The bEnd.3 cells were seeded 8000 cell/well to 8 well μ-slides (Ibidi). After 7 days, the cells were washed twice with PBS and incubated with the peptides in serum-free DMEM without phenol red (Gibco, Thermofisher). After peptide incubation, the cells were washed two times with cold PBS to remove membrane-bound fluorophores and fluorescent proteins.

Cell membrane and lysosomes were stained with 5 μg/mL CellMask™ Deep Red plasma membrane stain (Molecular Probes, Thermofisher) and 100 nM LysoTracker® Red DND-99 (Molecular Probes, Thermofisher), respectively, for 15 min after peptide addition.

In order to observe peptide trafficking, cells were incubated with 25 μg/mL transferrin from human serum Alexa Fluor® 568 conjugate for 15 minutes after peptide addition.

For inhibitory conditions the concentration and periods of incubation were similar to described in section II.3.3.

Cells were visualized in serum-free DMEM without phenol red (Gibco, Thermofisher) in an inverted confocal laser point-scanning Zeiss LSM 880 microscope equipped with Diode 405-30, DPSS 561-20 and HeNe 633 lasers and a temperature control incubator at 37°C with 5% CO_2 supply. Images were taken with Plan-Apochromat 20x dry objective and 63x oil objective (Zeiss). The Z-stacks images were obtained from the centre of the cell with a range of 14.05 μm. A total of 15 to 20 raw images were collected.

All images and co-localization analysis were performed with Fiji software (ImageJ v2.0.0).

III. RESULTS AND DISCUSSION

III. RESULTS AND DISCUSSION

III.1. Recombinant Protein GFP-Pep

In order to study the translocation mechanism of the cell-penetrating peptides (CPPs), two of the best studied peptides, Tat and Penetratin, along with our peptide of interest, PepH3[1], were conjugated with green fluorescent protein (GFP). Conjugation was performed by recombinant protein technologies, using PCR and followed by cloning in two similar expression vectors, pET28a (+) and pETM-10, to test which one would allow for a better protein expression.

pET28a (+) is a common expression vector employed with recombinant proteins expressed in bacteria, nevertheless new expression vectors have been developed to improve the yield of cloning and protein expression. pETM vectors are derived from pET (Novagene) and they share many common characteristics with pET vectors such as the His-Tag in the N-terminal, a protease recognition site and the conserved multiple cloning site (MCS). Studies have shown that pETM vectors can be employed in expedite protein production[64], due to their start with a NcoI recognition site allowing for a simultaneous digestion with two restriction enzymes without the need to exchange the digestion buffer as with pET28a (+) vector.

The first step was the amplification of GFP gene by PCR using a reverse primer that contains the peptide of interest, either Tat, Penetratin or PepH3. In order to confirm if amplification was successful, the samples were applied into an agarose gel and visualized under UV light. The resulting agarose gel is shown in Figure III.1. The positive control consisted of amplification of GFP gene using unmodified primers (lanes 4 and 7), and for the negative control the DNA was replaced by dH_2O (lanes 2, 5 and 8) and using the respective modified primers. In lane 3 we can see amplified Nhe-GFP-H3-Xho DNA while in lane 6 and 9 we can observe the amplified Nco-GFP-H3-Xho and Nco-GFP-Xho DNA, respectively.

[1] The PepH3 was designed with two different linkers. One linker is the same as the control (GFP-H3) while the other linker is equal to the Tat and Penetratin linker (GFP-sH3).

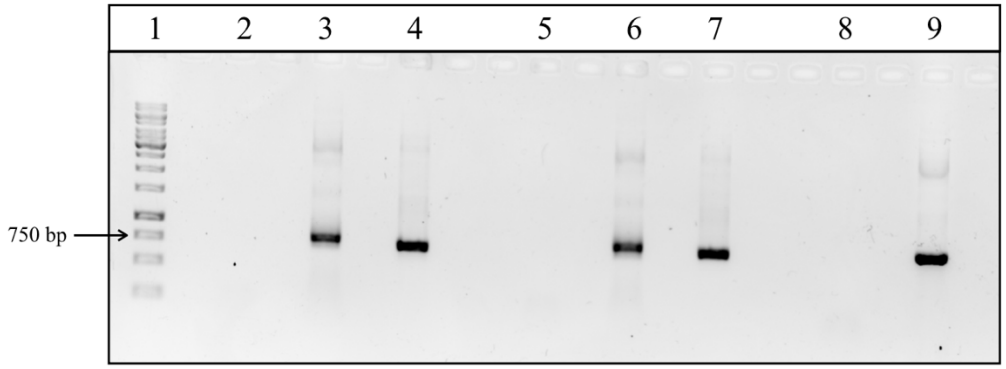

Figure III.1 - Inserts after PCR amplification in 2 % TBE agarose gel at 80 V. Lane: 1 – GeneRuler 1 kb DNA Ladder (Appendix VI.9); 2 – Nhe-GFP-H3-Xho Negative control (without DNA); 3 – Nhe-GFP-H3-Xho, insert for pET28a (+); 4 and 7 – Positive Control (Nhe-GFP-Xho); 5 – Nco-GFP-H3-Xho Negative control (without DNA); 6 – Nco-GFP-H3-Xho, insert for pETM-10; 8 – Nco-GFP-Xho Negative control (without DNA); 9 – Nco-GFP-Xho. 5 μL of each sample with 6x loading dye were loaded into each lane.

As seen in Figure III.1, the agarose gel of the PCR products depicts a band with 750 bp, similar to the positive control thus showing that amplification was successful. Also we can infer that the samples were not contaminated due to the absence of a band in the control lanes (lane 2, 5 and 6). Next, the bands containing the DNA were purified with a gel extraction kit. The purified samples were digested, using the respective restriction enzymes, and purified using a PCR clean kit.

In order to clone the proteins, the amplified and digested DNA fragments were ligated to cut pET28a (+) vector (restriction sites: NheI an XHoI) and pETM-10 vector (restriction sites: NcoI an XhoI) in a 1:3 proportion. Next, the plasmids were transformed in *E. coli* competent cells: dH5α cells for a good DNA propagation and maintenance; and BL21(DE3) cells for protein expression. For negative control no colonies were observed, while for clones at least fifty colonies were counted.

To confirm that the transformation in dH5α cells was successful, four random colonies were picked and re-suspended in dH_2O for PCR amplification. After confirmation of clones by electrophoresis in an agarose gel, the samples were sent for sequencing. Subsequently, employing the Basic Local Alignment Search Tool (BLAST) the sequencing results were compared with expected nucleotide sequence that will produce the protein of interest, GFP, GFP-H3, GFP-sH3, GFP-Tat and GFP-PTT. The positive results were transformed into BL21(DE3) cells.

III.1.1. Expression and detection of target protein

Cells were grown at 37ºC until an $OD_{600} \cong 0.6$ was reached and induced with 0.6 mM IPTG. Aliquots were taken at different stages of growth: immediately before cell induction (0 hours) and 3, 6 and 24 hours after induction. After each time, the samples were prepared to obtain the different cellular fractions: total, soluble and insoluble cellular fraction. The total fraction comprises the pellet that was obtained after centrifugation of the initial sample. After resuspension of the pellet in binding buffer and centrifugation two fractions were obtained: the soluble (supernatant) and insoluble (pellet) fractions. All fractions were analysed by SDS-PAGE electrophoresis to detect target proteins. Figure III.2 shows the resulting SDS-PAGE gel.

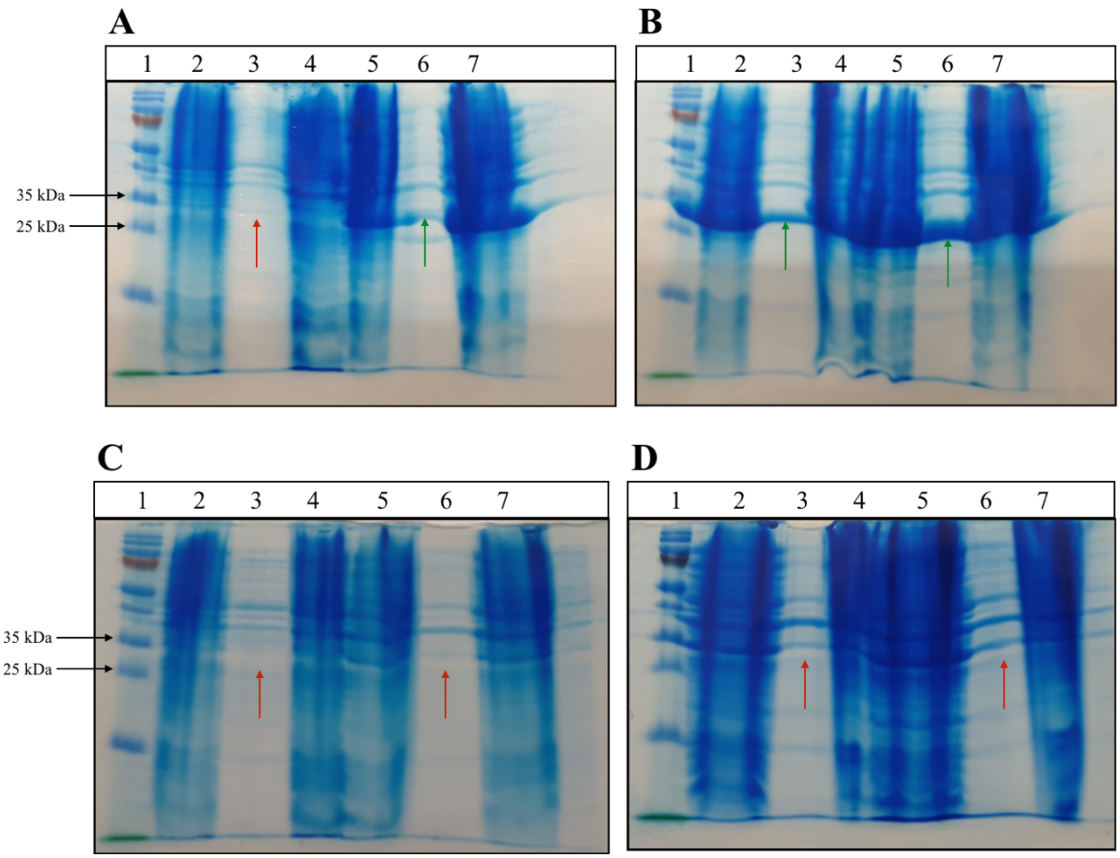

Figure III.2 - Fractions collected of pET28a-GFP (A and B) and pETM10-GFP (C and D), SDS-PAGE 12%, 180 V. A and C: 1 – Protein Ladder, 2 – Total fraction t=0h, 3 – Soluble fraction t=0h, 4 – Insoluble fraction t=0h, 5 – Total fraction t=3h, 6 – Soluble fraction t=3h, 7 – Insoluble fraction t=3h; B and D: 1 – Protein Ladder, 2 – Total fraction t=6h, 3 – Soluble fraction t=6h, 4 – Insoluble fraction t=6h, 5 – Total fraction t=24h, 6 – Soluble fraction t=24h, 7 – Insoluble fraction t=24h. The green and red arrows indicate where, in the soluble fraction, the interest proteins are expected based on their apparent molecular weight.

The SDS-PAGE gels on Figure III.2 show the different fractions collected at different stages of GFP expression in the two different expression vectors employed, pET28a (+) (Figure III.2 A and B) and pETM-10 (Figure III.2 C and D). The total fraction is composed by the total cellular

extract. After cell lysis there are two fractions: the soluble fraction that encompasses cytoplasmic, periplasmic and membrane proteins and the insoluble fraction comprised by cellular debris and inclusion bodies. As GFP is a 27 kDa protein its band should appear between the 25 and 35 kDa bands from the protein marker. For both expression vectors, at the initial time (t=0h), there is no band in this molecular range. This situation was already anticipated since the induction of the interest protein with IPTG had just occurred. Over time, for the expression in pET28a (+) vector, it is possible to observe a band with a compatible apparent molecular mass in all fractions, including the soluble ones. Also, over time, expression in the pETM-10 vector yielded a GFP that could only be found in the total and insoluble fractions. As GFP is only found in these fractions, seems that this protein is in the inclusion bodies.

The literature describes that the pETM vectors are designed for rapid subcloning expression and subsequent purification. However, our results show the opposite at least for GFP protein. As the protein is in the inclusion bodies, the purification process becomes more complex and time consuming. Therefore, pET28a (+) is a better vector to express GFP and consequently, their conjugates. So, pET28a (+) was the vector chosen to express the proteins.

III.2. GFP-pep purification

As a large quantity of pure GFP and GFP-pep was necessary for carrying out the cellular and microscopy assays, it was necessary to express both proteins in large scale. To achieve the necessary amount of protein the cells were grown in 500 mL SB medium, supplemented with kanamycin and induced with IPTG, at 25°C for approximately 20 hours. Then, the cells were harvested by centrifugation and lysed by sonication. The lysate was cleared by centrifugation and a 25 mL soluble fraction was obtained. Next step was to purify the proteins of interest present in the soluble extract. As these proteins have an exposed histidine tag, it allowed them to be purified by Metal-Chelate Affinity Chromatography (MCAC) using a 5 mL HisTrap column. First, the protein extract was washed with 50 mM sodium phosphate buffer containing 1 M NaCl and 10% glycerol at pH 6.8 (buffer A) to remove the proteins that did not adsorbed. Then a discontinuous linear gradient of 4 column volumes, with 50 mM sodium phosphate, 1 M NaCl, 500 mM imidazole and 10% glycerol at pH 6.8 (buffer B) was employed to elute the proteins of interest. To monitor protein elution, the absorbance was measured at 395 nm, corresponding to the wavelength of the first absorbance pick of GFP. The chromatograms depicting the protein elution profiles are displayed in Figure III.3.

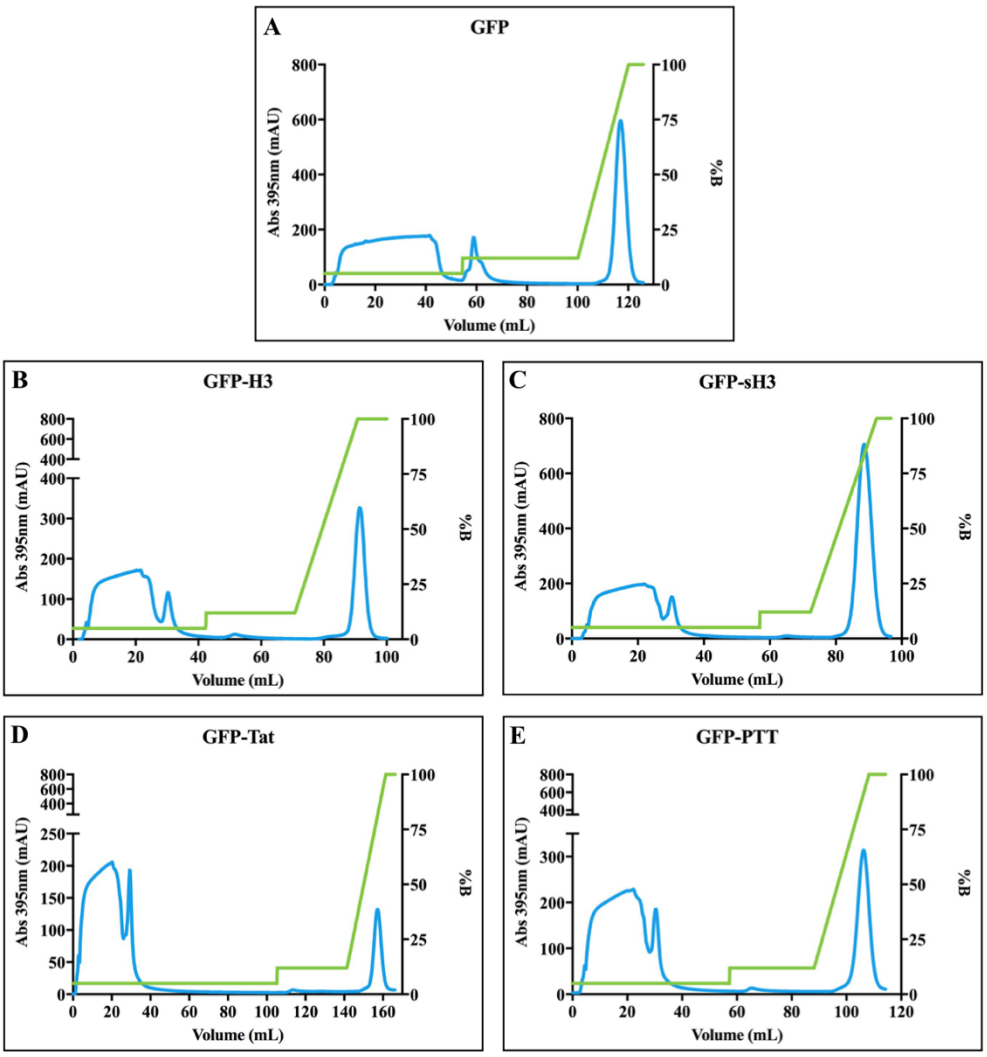

Figure III.3 - Elution profile of the protein purification in His-Trap 5 mL column. **A:** GFP, **B:** GFP-H3, **C:** GFP-sH3, **D:** GFP-Tat, **E:** GFP-PTT; the blue line represents the absorption at 395 nm and the green line the percentage of B buffer that composes the mobile phase. The work flow was 1 mL/min.

After MCAC purification, the collected fraction was injected in a molecular exclusion column to further purify it and to ensure protein stability. Protein elution was performed with PBS containing 1mM DTT using a HiLoad 16/60 Superdex S200 column at a flow of 1 mL/min. The eluate absorbance was monitored at 280 nm and 395 nm. The chromatograms of protein elution profile in Superdex S200 column are display in Figure III.4.

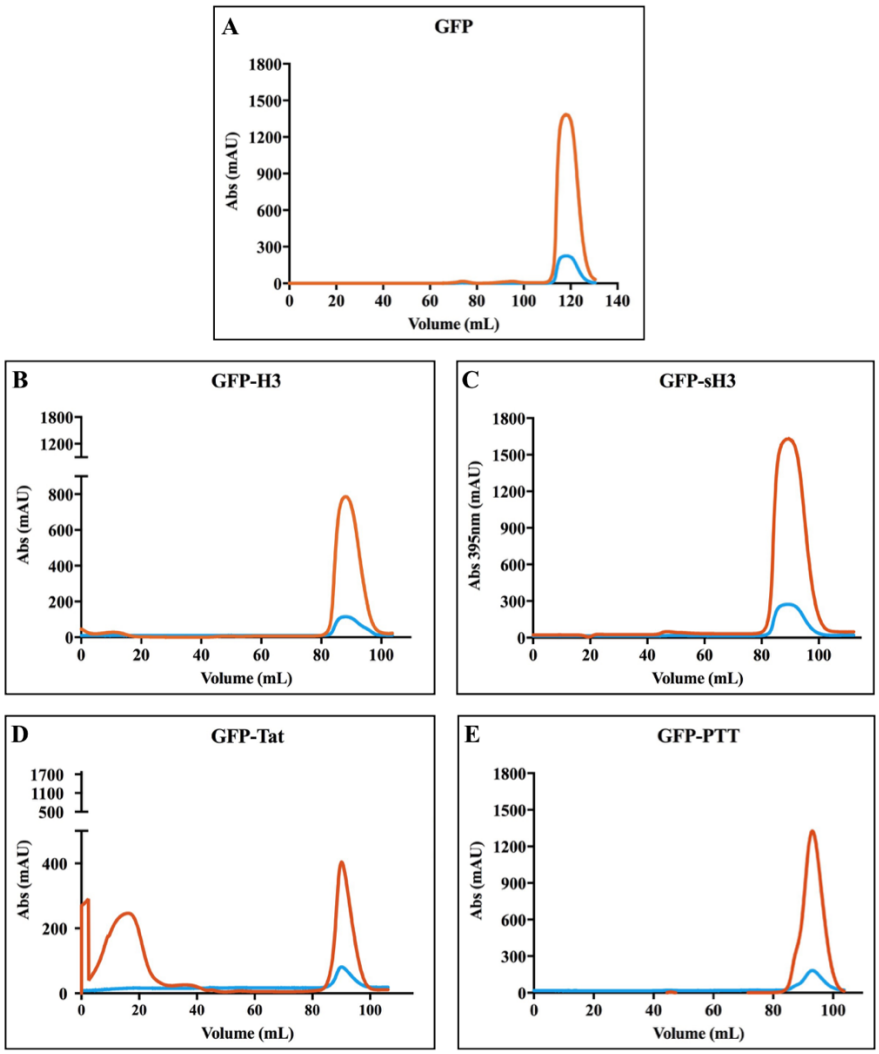

Figure III.4 - Elution profile of the protein purification in a Superdex S200 column. **A:** GFP, **B:** GFP-H3, **C:** GFP-sH3, **D:** GFP-Tat, **E:** GFP-PTT; the blue line represents the absorption at 395 nm and the orange line the absorption at 280 nm.

After the molecular exclusion chromatography, the fractions collected were pooled and a total volume of 15 mL was retrieved. Protein samples were concentrated and quantified by two different methods. In the first method a Nanodrop spectrophotometer was employed and protein concentration was determined by measuring the absorbance at 280 nm and employing the corresponding extinction coefficient and molecular weight obtained through the ProtParam Database by diluting the samples with PBS with 1mM DTT in a 1:2 ratio. The second method employed was a traditional Bradford protein assay. Quantification results are showed in Table III.1.

Table III.1 - Protein quantification by Nanodrop and Bradford methods after purification and concentration. ε and MW were calculated with ProtParam.

Sample	ε ($M^{-1} cm^{-1}$)	MW (Da)	Quantification by Nanodrop (mg/mL)	Quantification by Bradford (mg/mL)
GFP	21890	26954.4	17.18	17.82
GFP-H3	27390	29735.3	3.94	3.77
GFP-sH3	27390	29332.9	20.26	14.47
GFP-Tat	21890	30208.9	2.86	2.85
GFP-PTT	32890	30966.8	8.58	6.38

The protein quantification results are similar in both methods, exception made for the quantification of the GFP-sH3 protein where a greater difference between both methods can be observed. Whereas the Nanodrop quantification is based solely on the Lambert-Beer equation (Absorbance (A) = Extinction coefficient (ε) x path length (b) x analyte concentration (c)) that correlates absorbance with concentration, the Bradford assay is also more susceptible to the amino acid composition of the quantified protein. This method is more susceptible to interference by various chemicals that may be present in the protein sample.

However, we can see that the quantifications are in line with the chromatographic results obtained in the purification step, as we can observe a higher peak at 280 nm in the case of GFP-sH3, corresponding to a greater amount of protein while GFP-Tat has the lowest peak at 280 nm, corresponding to a lower protein quantity.

Figure III.5 shows the electrophoretic profile of the purified protein obtain through SDS-PAGE performed with equal concentrations of protein, 15 μg/μL. We can observe a single band for each protein, thus we can conclude that the interest proteins were successfully purified. We can also observe that the GFP-Tat and GFP-PTT (lane 2 and 3, respectively) have a similar molecular weight (30.21 and 30.97 kDa, respectively) while the GFP-sH3 and GFP-H3 (lane 4 and 6, respectively) have a slightly lower one (29.33 and 29.74 kDa, respectively) and also, by observation of lane 5, that GFP that is the lightest of all purified proteins (26.95 kDa).

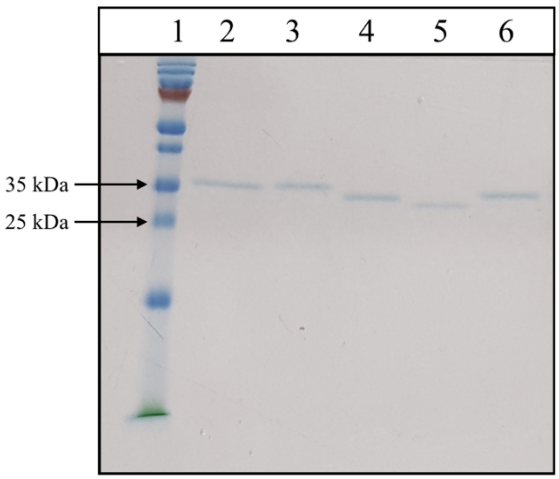

Figure III.5 - SDS-PAGE from the pure protein collected after all chromatographic steps and concentration; 20 µL of each sample were loaded into each lane of a 12 % polyacrylamide gel. **Lanes: 1 -** PageRuler Prestained Protein Ladder; **2 -** GFP-Tat; **3 -** GFP-Ptt; **4 -** GFP-sH3; **5 -** GFP; **6 -** GFP-H3.

III.3. GFP-pep interaction with Brain Endothelial Cells

Cell-penetrating peptides are being considered promising new tools for drug delivery. This part of the work, was dedicated to the test of peptides that were previously conjugated with GFP in bEnd.3 model cell to understand which of the main mechanisms is used by PepH3 to translocate BBB and what are the effects its translocation has on the cells.

III.3.1. Preliminary GFP-pep translocation studies

Before starting the translocation assays it was necessary to optimize the conditions performed. In particular, peptide concentration and their incubation time. Therefore the selected concentration range for these assays covered the peptide concentration used in these types of experiments, normally in the nM or μM range. As a cellular model system, we selected bEnd.3 cells because this immortalized mouse brain endothelial cell line can establish barrier characteristics, including complex tight junctions, in a more expedite way.

The bEnd.3 cells grown in the apex of tissue cultured inserts were incubated with four different concentrations of GFP-H3, 0.05, 0.1, 1 and 10 μM in Transport buffer (1 M glucose, 1 M $MgCl_2$, 1 M HEPES, 3% BSA and PBS) at 37°C with 5% CO_2. The Transport buffer is employed to simulate the physiological conditions. After, 15 min, 5 and 24 hours, the samples were collected from the apex and base of the cell culture plates. Cellular uptake was quantified by fluorescence spectroscopy. The fluorescence signal of samples was obtained exciting the GFP at 395 nm and recording its emission at 509 nm. Figure III.6 shows the quantification results for different concentration of GFP-H3 with different time points.

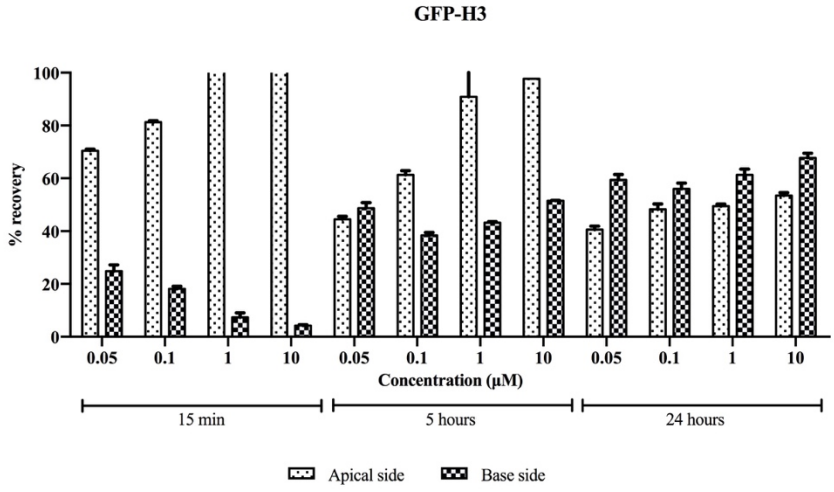

Figure III.6 - Concentration and time dependence of GFP-H3. The graph shows the percentage of different GFP-H3 concentrations in apex and base side at different time points. Error bars represent the standard error of the mean (SEM) from triplicates.

For different time points, it is possible to observe an increase in the amount of peptide over time, mainly after 24 hours where it is possible to observe a higher percentage of GFP-H3 in the base. However, after cells observation with an optical microscope (data not shown) it was detected that the cellular barrier was destroyed by the 24-hour time point, thereby allowing peptide translocation from the apex to the base. At the time point of 15 minutes the percentage of GFP-H3 translocation is not significant because most of the peptide is at the apex. This leads us to conclude that 15 minutes are not sufficient to allow for a significant amount of peptide to translocate the BBB. Also, with a lower peptide concentration and after a five-hour incubation it is possible to observe the peptide at both, the apex and the base. It is also showed that for a higher peptide concentration, the translocated percentage is approximately 45%. Which is similar to the one obtained employing lower peptide concentrations. However, for higher peptide concentrations its percentage in the apex is much higher than expected, greater than 95%, as for the 15 minutes time point. Probably, at higher concentrations, the peptide tends to aggregate among themselves leading to an increase in the fluorescence signal. After 24 hours this does not happen because the monolayer barrier is destroyed allowing for the passage of such peptide aggregates.

So, for the next assay, cells were incubated for 30 minutes, 5 and 10 hours, at 37°C, 5% CO_2 in transport buffer with 0.1 μM of GFP and their conjugates.

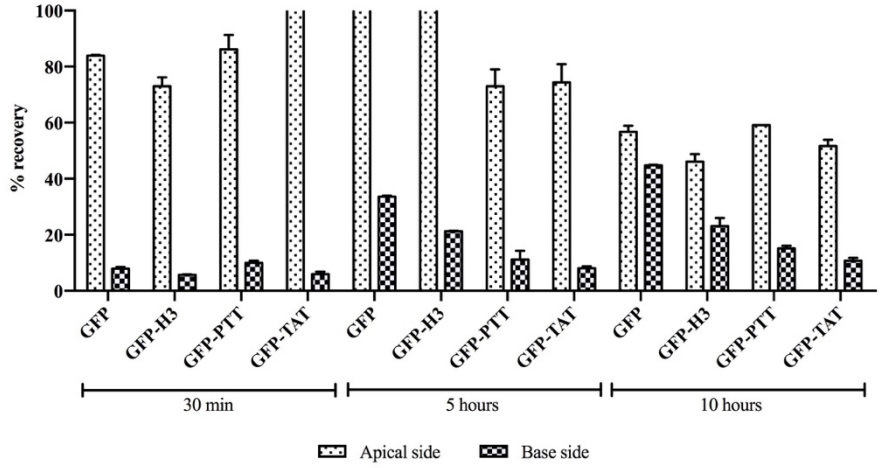

Figure III.7 - Time dependence of 0.1 μM GFP and their conjugates. The graph shows the percentage of different GFP-conjugates in apex and base side at different time points. Error bars represent the SEM from triplicates.

Figure III.7 shows the recovery percentage of the GFP and GFP-peps at 30 minutes, 5 and 10 hours. As before, the quantity of peptide that translocated tends to increase over time, as it is possible to find a significant percentage of peptide in the apex side after 30 minutes but, after 10

hours the largest percentage of peptide is in the base side. However, once more, after 10 hours, the cells were once more observed under the optical microscope (data not shown) and it was found that the cellular barrier had been destroyed.

The peptide uptake percentage is influenced by the conditions in which the cells are grown and their ability to form a tight junctions' monolayer. So, in these assays it was extremely important to control cellular integrity and to understand the mechanism responsible for their instability. Thus, the cells were incubated with 0.1 μM of peptides in transport buffer at 37°C, 5% CO_2. After 5 hours the samples from the apex and base were collected and the cells were incubated again with FD40 (fluorescein isothiocyanate-dextran, 40 000 Da) in transport buffer, for 2 hours at 37°C, 5% CO_2. FD40 is a 40 kDa fluorescently labelled dextran that is commonly used to monitor paracellular permeability. This probe had an initial concentration of 25 mg/mL and sequential dilutions were done until an absorbance of 0.1 or lower was achieved before adding it to the apex. All collected samples were analysed by fluorescence spectroscopy, for GFP samples the fluorescence signal was obtain as previously described, while the FD40 signal was obtained exciting the samples at 493 nm and recording its emission at 560 nm.

Figure III.8 shows the results of the translocation assay with peptides incubated for 5 hours at 37°C and cellular integrity with FD40 during 2 hours.

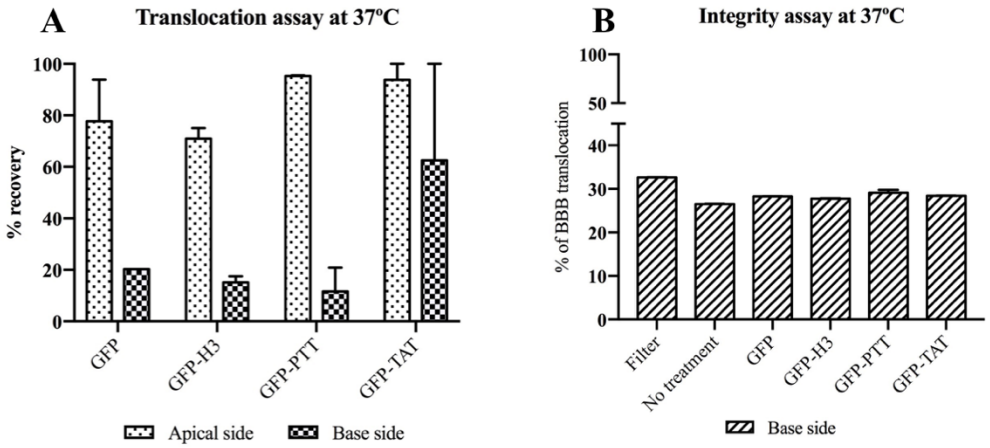

Figure III.8 - Translocation and integrity assay of different peptide conjugates in transport buffer. **A –** Translocation assay at 37°C; shows the percentage of peptide recovered at apex and base after 5 hours of incubation with 0.1 μM of the different conjugates. **B –** Integrity assay at 37°C; shows the percentage of BBB translocation by FD40 probe. Filter is a control without cells and No treatment is a control where the cells were incubated with transport buffer. Error bars represent the SEM from triplicates.

The results in graph A, Figure III.8, show that the percentage of peptide recovered from the base side is similar to the one obtained in the assays shown in Figure III.7. The only exception is for the recovered percentage of GFP-Tat where that is greater on the base side. To validate the

results of the translocation assay it is important to observe the cellular integrity after cell incubation with the peptide. Graph B of Figure III.8 shows the percentage of FD40 probe that was able to translocate the BBB. These results allow us to understand how integrate was the cell monolayer. To achieve two controls were prepared. The filter control results from the incubation of FD40 with transport buffer and does not contain cells, while the "no treatment" control contains cells that were incubated with transport buffer for 5 hours and then with the FD40 probe. The results of the cellular integrity assay show that cells incubated with different peptides have a similar translocation percentage to both, the cellular control sample - no treatment, and the control without cells, Filter. This being the case, the cellular integrity assay suggests that the cellular barrier was destroyed and consequently the results from the translocation assay cannot be considered valid since there is no barrier to translocate and consequently the peptides can easily traffic between sides.

In an attempt to explain these results two hypotheses were formulated. The first hypothesis was that the cellular barrier was destroyed by either the incubation medium or the transport buffer. The second hypothesis was that the cellular barrier was compromised by the peptides as the cell penetration properties of CPP delivery agents might be depend on the associated cargo. In this case, the CPPs cargo is GFP, a high molecular weight protein that some studies state as having the capacity to deliver peptides into mammalian cells. However, in previous results we observed that the percentage of GFP translocation is greater than that of GFP-peps. Therefore, there is the possibility that the GFP is inducing the peptide translocation and not the other way around, as was expected. As the GFP might be the first to interact with the cell membrane, it may be perturbing the membrane leading to its destruction;[65] The first hypothesis is the most likely since the percentage of translocation of the FD40 probe in untreated cells is close to that of the control without cells.

Subsequently, to test the first hypothesis, the GFP and its conjugates were diluted in complete DMEM culture medium (with Pen Strep and 10% FBS) to stabilize the cultured cells. These were incubated with 0.5 μM of GFP and GFP-peps for 5 hours at 37°C, 5% CO_2. After sample collecting the cells were incubated with FD40 probe also diluted with complete DMEM culture medium.

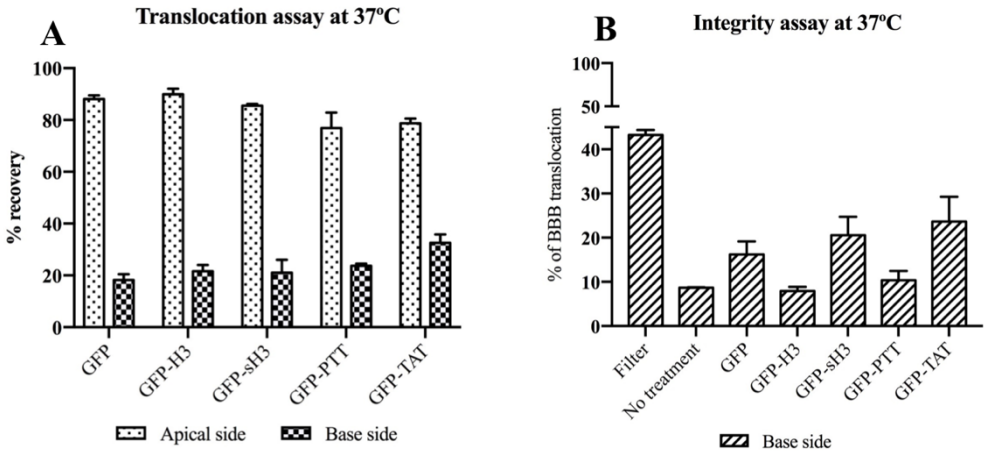

Figure III.9 - Translocation and integrity assay of different peptide conjugates in complete DMEM. **A -** Translocation assay at 37°C; shows the percentage of peptide recovered at the apex and base after 5 hours of incubation with 0.5 μM of the different conjugates. **B -** Integrity assay at 37°C; shows the percentage of BBB translocation by the FD40 probe. Filter is a control without cells and "No treatment" is a control where the cells were incubated with complete DMEM. Error bars represent the SEM from triplicates of at least two independent experiments.

After performing the translocation assay in complete DMEM instead of transport buffer, we can observe a considerable improvement in cell integrity (Figure III.9 B), as the percentage of FD40 that translocates the BBB, in the "no treatment" sample, is considerably lower (8.66% ± 0.18) when compared to the percentage of translocated FD40 on the sample without cells (43.24% ± 2.27). Therefore, it can be assumed that the incubation in transport buffer was damaging the cellular barrier.

Figure III.9 A, shows the recovery percentage of the different peptides after a 5-hour incubation. Earlier, we hypothesised that the GFP might be maximizing the peptide translocation and not the opposite, as expected. However, these results show that the conjugates have a higher translocation percentage when compared to the translocation percentage of GFP alone, thus we can reason peptides may have a lead role in the cellular translocation of their cargo. Nonetheless, reviewing the results of the cellular integrity assay, it is possible to observe that the percentage of FD40 that translocates the BBB is higher for the GFP sample than it is for the "no treatment" control, which may indicate that the amount of GFP translocated thought the cells might be due to the formation of gaps between them. The only samples that display an integrity considered good are the GFP-H3 and GFP-PTT conjugates as they exhibit similar results to the "no treatment" control, while the other samples display results that are characteristic of cells that are not arranged in a cellular monolayer (Figure III.9 B).

Comparing the results obtained during the translocation assays (Figure III.9 A) for GFP-H3 and GFP-sH3, we can observe that the BBB translocation percentage between them is similar, 21.63% ± 4.81 and 21.01% ± 7.51, respectively. However, when we observe the results of the

integrity assay for both samples, we can see that the cells incubated with GFP-H3 present a better integrity than ones incubated with GFP-sH3, showing that in this case, the linker has an influence on BBB translocation. As described in Chapter I.4, CPPs characteristics such as their sequence, size, charge, structure and stability as well as the characteristics of their cargo such as its structure or charge can also contribute for their translocation and studies suggested that the spacer linker can also contribute to the translocation of the CPP.[49] The PepH3 is composed by seven amino acids and is linked by twelve amino acids to form the conjugate GFP-H3, while the GFP-sH3 linker is composed by six amino acids. When the PepH3 is conjugated with GFP employing a short linker its sequence is very short and the conjugate has a BBB translocation percentage similar to that of the GFP-H3 peptide, however, as shown by the integrity assays it also perturbs the cell monolayer because the percentage of FD40 that translocates the BBB is higher for the GFP-sH3 than it is for the "no treatment" control. When the PepH3 is conjugated with the bigger linker, it can interact with the cellular membrane and cross the BBB without toxic effects as in the B graph of Figure III.9 the FD40 percentage that translocates the BBB is lower for the GFP-H3 than it is for the "no treatment" control. The translocation assay (Figure III.9, graph A) also demonstrated that the GFP-PTT and GFP-Tat have a higher translocation percentage when compared to the translocation percentage of GFP-H3 (23.66% ± 3.63 and 32,61% ± 9.68, respectively). However, the integrity assay also shows, in Figure III.9, B graph, that the GFP-Tat induces a higher perturbation to the cell monolayer then the GFP-PTT, as the cells incubated with this peptide displayed a cellular integrity similar to that of the "no treatment" control.

The objective of the CPP, PepH3, is to cross the BBB. However, the CPP may fail to cross it, because it might be retained by the cell membrane or because they may remain enclosed inside the cells. To assess if any of these cases occurs, cellular interaction and internalization assays were performed. For these assays bEnd.3 cells grown in culture plates, were incubated with conjugates in the same conditions described for the translocation assays. After 5 hours, the medium was collected to simulate the apical side. This collected medium contains the free conjugates that were not enclosed inside the cells or did not interact with the cell membrane. Then, to recover the protein membrane interaction samples, the cells were washed with cold PBS followed by an acid buffer (100 mM NaCl and 50 mM Glycine, pH 2.8) and once again with PBS. Next, the cells were lysed using RIPA buffer (50 mM Tris-HCl, 150 mM NaCl, 1% Triton X-100, pH 7.2) and the soluble proteins were cleared by centrifugation to recover the peptide that was retained inside the cell. Quantification was performed by fluorescence spectroscopy just like in the previous experiments. Figure III.10 shows the results of cellular interaction and internalization assays.

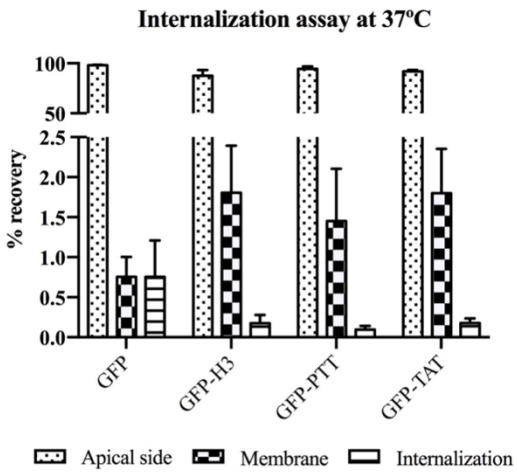

Figure III.10 - Cellular interaction and internalization of different peptide conjugates in a 0.5 μM concentration in complete DMEM at 37°C. Results show the percentage of peptide recovered in a culture plate chamber after 5 hours of incubation with 0.5 μM of the different conjugates. Subsequently, the incubation medium was removed and with it the free peptide. Then cells were washed to recover the peptides that interacted with the cellular membrane. Finally, the cells were recovered and lysed and the peptide that was retained inside them was recovered. Error bars represent the SEM from triplicates of at least two independent experiments.

The results of the cell membrane interaction and internalization are presented in Figure III.10. It is possible to observe that the majority of the conjugates, over 90%, are found in the culture medium. This is very important, because CPPs aggregation occurs mainly in the cell membrane[37] thus, this assay was performed to verify if there was a significant amount of peptide that interacts with the cellular membrane without cross it. Figure III.10, shows that in what concerns the percentage of peptide that interacts with the cellular membrane the GFP-H3 and GFP-Tat are the samples that displays a higher percentage of peptide interaction, about 1.81% ± 1.17 and 1.80% ± 1.11, respectively, while GFP-PTT show 1.45% ± 1.30 interaction with the cellular membrane. It is also possible to observe that GFP displays the lowest percentage of interaction with the cellular membrane and only, 0.76% ± 0.50 of GFP interacts with the cellular membrane. In contrast, GFP without peptide is the protein that shows the higher internalization values, 0.8% ± 0.13 but, when GFP is conjugated with peptides the accumulation inside the cells was relatively low, less than 0.18%. These results suggest that these peptides can cross the BBB with their cargo without being retained in the cellular membrane or inside the cells. Neves *et al*, also showed that PepH3 does not associate to membrane proteins of bEnd.3 cells, hypothesising that the translocation mechanism of this peptide might be of an adsorptive-mediated transcytosis type. However, this hypothesis could only be tested with additional assays resorting, for example, to the use of specific inhibitors.

III.3.2. Metabolic inhibition studies

A systematic analysis of intracellular transport pathways can be achieved by analysing the effects of inhibiting one or more transport processes. To inhibit energy-dependent transport a temperature block can be applied. To perform these assays, bEnd.3 cells were incubated with 0.5 μM of GFP and GFP-peps in complete DMEM for 5 hours at both 37°C and 4°C. Figure III.11 shows the translocation and integrity assays for the different peptide conjugates at 4°C while the results obtained after an incubation at 37°C were presented in Figure III.9.

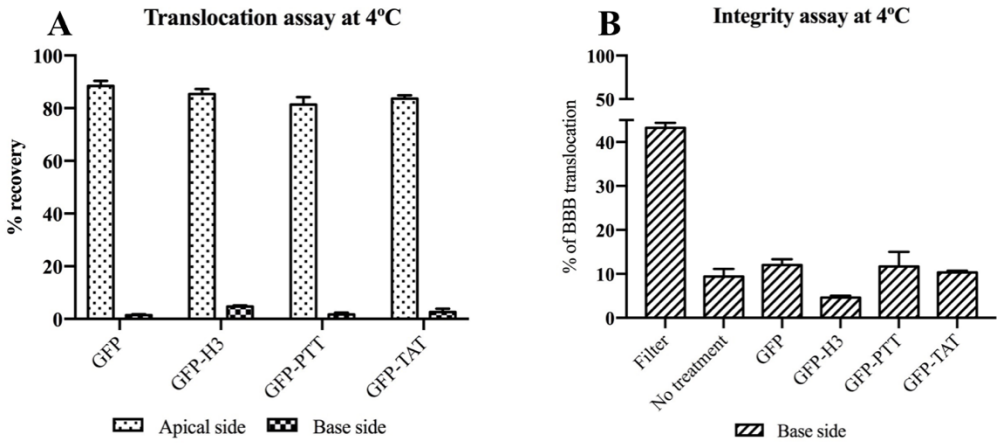

Figure III.11 - Translocation and integrity assay for different peptide conjugates in complete DMEM at 4°C. **A -** Translocation assay at 4°C, shows the percentage of peptide recovered at the apex and base after 5 hours of incubation with 0.5 μM of the different conjugates. **B -** Integrity assay performed at 4°C showing the percentage of BBB translocation by FD40 probe. Filter is a control without cells and No treatment is a control where the cells were incubated with complete DMEM. Error bars represent the SEM from triplicates of at least two independent experiments.

In Figure III.11 A, it is possible to observe that the percentage of recovered peptide from the base side is less than 5% for all peptides. Comparing these results with the results obtained at 37°C (Figure III.9 A) there is a considerable decrease in the peptide quantity that is able to cross the cells. In the particular case of our interest peptide, PepH3, the percentage of peptide recovered in base side decreases from 21.63% ± 4.81 to 4.63% ± 0.79. These results demonstrate that the peptide translocation is inhibited at low temperatures, thus in this stage we can propose that the peptide translocation mechanism is energy-dependent.

The results depicted in Figure III.11 B, shows that at low temperatures the cellular integrity is maintained because the results with FD40 for cells incubated with different peptides, are similar with the no treatment control. From the comparison of the integrity results at both temperatures (Figure III.11 B and Figure III.9 B), it is observable that the integrity at 4ºC is

better than at 37°C, thus demonstrating that in this conditions the peptides do not exhibit toxic effects.

Cellular interaction and internalization studies were also performed in an attempt to understand if the membrane interactions or peptide internalization is temperature dependent. These assay was performed as previously described but changing the temperature for 4°C.

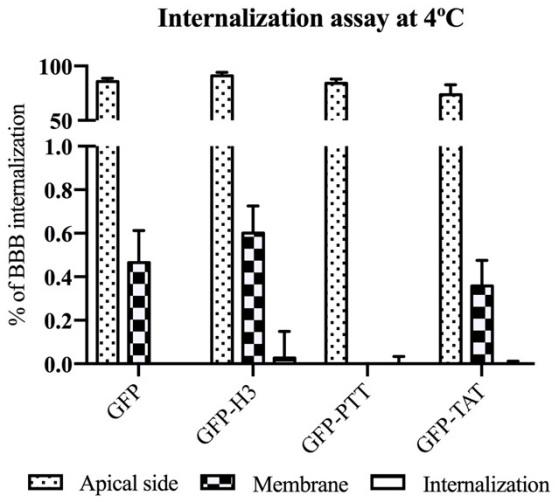

Figure III.12 - Cellular interaction and internalization of different peptide conjugates with 0.5 μM in complete DMEM at 4°C. The results present the percentage of peptide recovered in a culture plate chamber after a 5-hour incubation with 0.5 μM of the different conjugates. Subsequently, the incubation medium was removed and with it the free peptide. Then cells were washed to recover the peptides that interacted with the cellular membrane. Finally, the cells were recovered and lysed and the peptide that was retained inside them was recovered. Error bars represent the SEM from triplicates of at least two independent experiments.

In Figure III.12 it is possible to observe that over 90% of the peptides are found in the incubation medium and less than 0.6% are in the membrane while a nearly null percentage is inside the cells. The membrane interaction results are similar to the results obtained at 37°C but, the internalization values decreased at low temperature. So, these results suggest that the peptide internalization and translocation is inhibited by low temperatures and that the mechanism of translocation is energy-dependent.

III.3.3. Endocytosis inhibition studies

As described in Chapter I.4 the CPPs can cross the BBB by two principal systems, an energy-independent direct translocation or an energy-dependent endocytosis system. Nevertheless, we have shown that an energy-dependent mechanism allows for a better explanation of the results obtained.

Studies with CPPs[40,45] have shown that is very common for these peptides to be translocated employing several endocytic pathways belonging to the AMT systems. To further explore the possibility that PepH3 is able to translocate via an endocytic mechanism, we studied the effect of a collection of known endocytic inhibitors had in the peptides ability to translocate the cell membrane. Since our previous results show that GFP and GFP-Tat were disturbing the cell monolayer, it was decided to carry the endocytosis inhibition studies using GFP-H3 and GFP-PTT. For these assays, bEnd.3 cells were pre-treated with each inhibitor for 30 minutes prior to incubation with 0.5 μM GFP-H3 and GFP-PTT for 5 hours at 37°C, 5% CO_2 (Figure III.13 A). A cellular membrane integrity test was also performed for each assay and its results are shown in Figure III.13 B.

To inhibit individual endocytic pathways several pharmacological inhibitors were employed: EIPA (5-(N-ethyl-N-isopropyl)amiloride) was used to inhibit the macropinocytosis by blocking off the Na^+/H^+ exchange; Chlorpromazine (CPZ) is a cationic amphiphilic drug which prevents the formation of clathrin-coated pits by a reversible translocation of clathrin and its adapter proteins from the plasma membrane to intracellular vesicles, thereby inhibiting the clathrin-mediated endocytosis;[66,67] Methyl-β-cyclodextrin (MβCD) was used to interfere with the lipid raft/caveolin-mediated endocytosis because it has a high affinity for cholesterol and consequently, blocks the internalization of several ligands[67]; and Dynasore that acts as dynamin inhibitor. This protein is essential for clathrin-coated vesicle formation in endocytosis, as well as for ligand uptake through caveolae, so, by using dynasore it is possible to inhibit both mechanisms, the clathrin- and caveolin-mediated endocytosis.[68,69] Inside the cell, the vesicles that were formed can fused with early endosomes, that can interact with the Golgi apparatus. Lastly, Brefeldin A, a protein that disrupts the Golgi trafficking by blocking the formation of transport vesicles to and from the Golgi apparatus was employed to understand if these vesicles could be retaining the peptides inside the cell.[70]

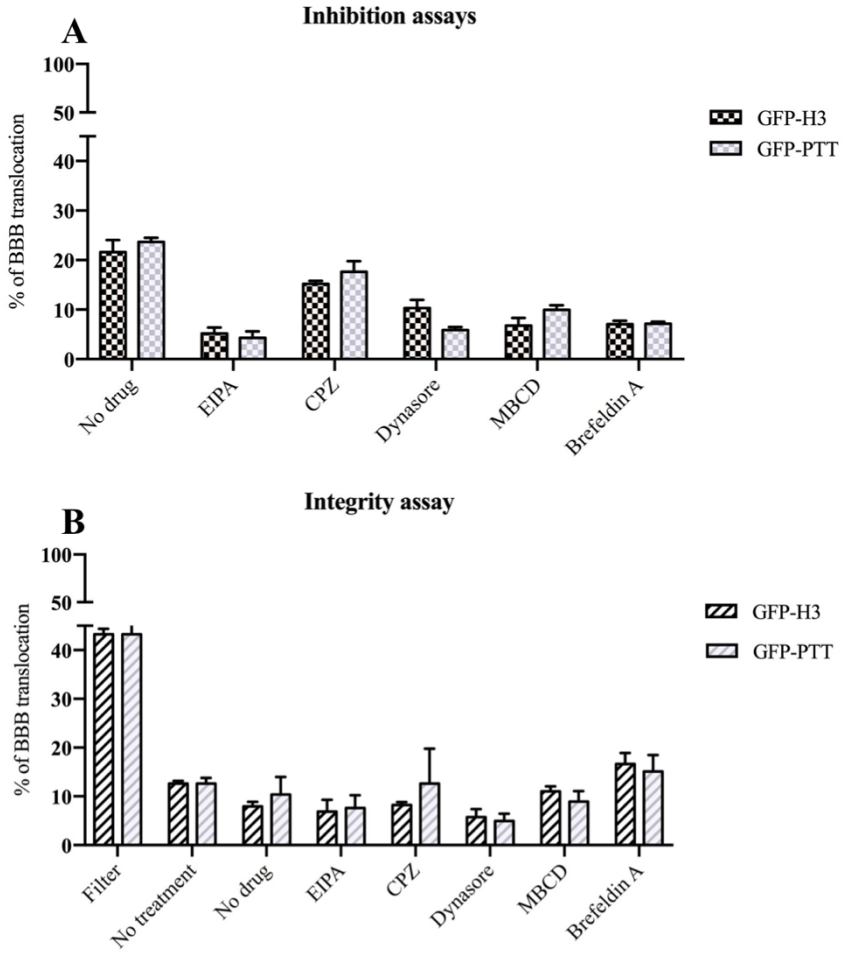

Figure III.13 - Inhibition and integrity assay of GFP-H3 and GFP-PTT in complete DMEM at 37°C. **A –** Inhibition assays where the cells were pre-treated for 30 minutes with the indicated inhibitor prior to a 5-hour incubation with 0.5 μM GFP-H3 and GFP-PTT. **B –** Integrity assay performed at 37°C showing the percentage of BBB translocation by FD40 probe. Filter is a control without cells and No treatment is a control where the cells were incubated with complete DMEM. Error bars represent the SEM from triplicates of at least three independent experiments.

Figure III.13, shows the influence of these inhibitors in peptide translocation. In general, it is possible to visualize a decrease in the peptide percentage in the base side and, although the percentages between inhibitors are similar, there are some differences between them. As previously described dynasore can inhibit two of the main routes leading to peptide translocation, clathrin- and caveolin-mediated endocytosis. When the cells were pre-treated with 50 μM of dynasore the peptide translocation percentage in base side decreases from 21.63% ± 4.81 to 10.34% ± 3.24 thereby indicating that dynamin might play an important role in the translocation mechanism of PepH3. However, analysing the two routes individually, the results show that with 50 μM of CPZ inhibitor the peptide translocation percentage decreases from 21.63% ± 4.81 to 15.19% ± 1.22. This decrease is not significant, suggesting that the peptide does not cross the BBB via clathrin-mediated endocytosis. In contrast, when the cells were pre-treated with 5 mM of MβCD the peptide translocation percentage decreases to 6.75% ± 3.08.

Regarding cell integrity (Figure III.13 B) it is possible to ascertain that the cell monolayer may have been disrupted, allowing for some of the peptide to translocate. It is also possible to infer that the caveolin-mediated endocytosis mechanism might be a favoured as there is a more significant decrease in the peptide translocation percentage. It is also possible to observe a decrease in the peptide translocation percentage of the cells that were incubated with 100 μM of EIPA, from 21.63% ± 4.81 to 5.20% ± 2.40. This observation indicates that the peptide might be translocating using the macropinocytosis internalization mechanism as excepted, since this is the principal mechanism by which macromolecules internalization occurs. Finally, when the cells were incubated with 10 μg/mL of Brefeldin A it was possible to observe that the peptides should get from the apex to the base side where it is only possible to recover 7.05% ± 1.43 of peptide. This decrease in the peptide translocation percentage may be an indication that the peptide's translocation mechanism is dependent on the formation of vesicles.

So, to confirm all these hypothesis further specific studies are required to establish a mechanism of translocation for these peptides.

III.4. Cellular pathway of peptide transmigration – Microscopy Studies

To confirm that the peptide was internalized, its uptake and intracellular localization were monitored by live cell image in confocal microscopy.

III.4.1. Preliminary microscopy studies

To determine the best conditions to perform the microscopy studies, the peptide was first analysed using a wide-field microscope. This is a simple and fast system that allows visualization of peptide internalization.

First, bEnd.3 cells grown in 8 well µ-slides were incubated for 15 minutes, 2 and 5 hours with 0.1 µM GFP-H3. After these time points, the cells were visualized with a Zeiss Axiovert 200M wide-field fluorescence microscope equipped with a green BP filter.

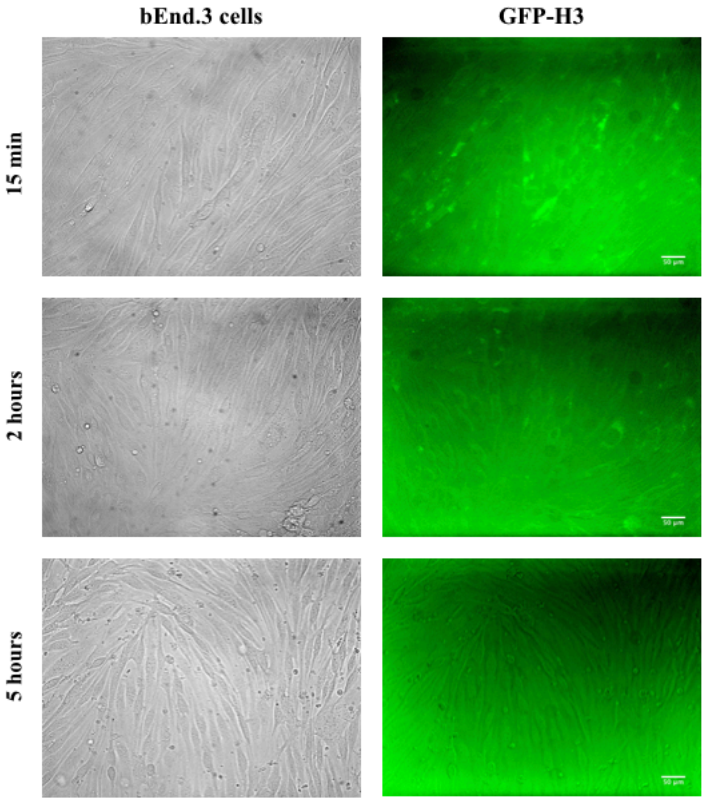

Figure III.14 - Live bEnd.3 cells incubated with 0.1 µM GFP-H3 for 15 minutes, 2 and 5 h at 37ºC. Images were obtained with a Zeiss Axiovert 200M wide-field fluorescence microscope equipped with a Green BP filter (Excitation: 450 – 490 nm and Emission: 515 – 565 nm). The scale bars represent 50 µm.

In fluorescence microscopy we recovered the signal emitted by fluorescence probes such as, in this case, the GFP. In none of the times points that were tested (Figure III.14) was possible to record a signal due to a significant background signal.

This situation might be due to a large concentration of the peptide in the media causing a "green carpet" effect. In an attempt to solve this problem wells were washed with PBS and fresh media was added. Nonetheless the problem remained and only for 15 minutes and 2 hours' time points was possible to visualize some peptide cellular internalization (Figure III.14). Another possible explanation can be linked to auto-fluorescence from the media. DMEM contains phenol red and riboflavin, and when excited they fluoresce in the same spectral range as GFP. Changing these parameters during the optimization process, it was found that the wide-field system is unsuitable for our experiments since the auto-fluorescence problem remained (data not shown). As described in Chapter I.5.4 the wide-field microscope capture all of the light emitted by sample, including light from outside of the focal plane, resulting in a significant amount of the signal being due to emitted background light and consequently auto-florescence. In contrast, the confocal microscope uses a pinhole that focuses a spot of light that is centred in the focal plane to eliminate out-of-focus light resulting in images of a greater clarity. Thus, the following experiments were performed in an inverted confocal laser point-scanning Zeiss LSM 880 microscope.

In following experiments, prior to peptide incubation in serum-free DMEM without phenol red, the bEnd.3 cells were washed twice with PBS to remove the residues of complete DMEM. After peptide incubation, the cells were washed again with cold PBS to remove membrane-bound fluorescent proteins and the images were obtained in serum-free DMEM without phenol red.

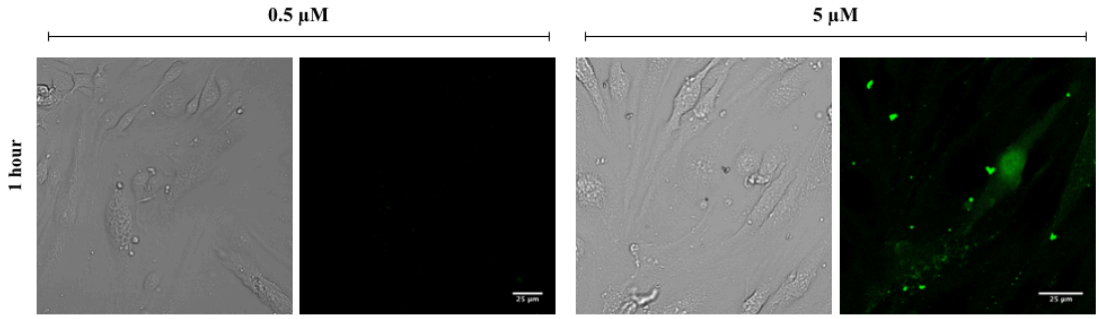

Figure III.15 - Assays for the determination of the protein concentration necessary to achieve a good fluorescence signal. Live bEnd.3 cells were incubated with 0.5 µM (Left images) and 5 µM (right images) of GFP-H3 for 1h at 37ºC, 5 % CO_2. Images were obtained by Z-stack (7/14) by Zeiss LSM880 microscope with a 488 nm laser and a 20x objective. A temperature control incubator was employed at 37°C with a 5 % CO_2 supply. GFP signal is recorded in green. The scale bar represent 25 µm.

To determine protein concentration necessary to achieve a good fluorescence signal in confocal microscopy assays, the same peptide concentration used in the BBB translocation model assays was tested. However, as shown in Figure III.15 no fluorescence signal was detected when the cells were incubated with the lower peptide concentration (images on the left). Thus, peptide concentration was increased to 5 µM for which was possible to record a

good fluorescence signal (Figure III.15, images on the right). In addition, using the confocal microscope improved the imaging, reducing the effect of the auto-florescence observed for the wide-field microscope.

With the objective of understanding how the peptide traffics through the cell, bEnd.3 cells were incubated for 1, 2 and 4 hours with 5 µM of GFP-H3 and then a microscopy assay was performed to check the location of the peptide within the cell over time.

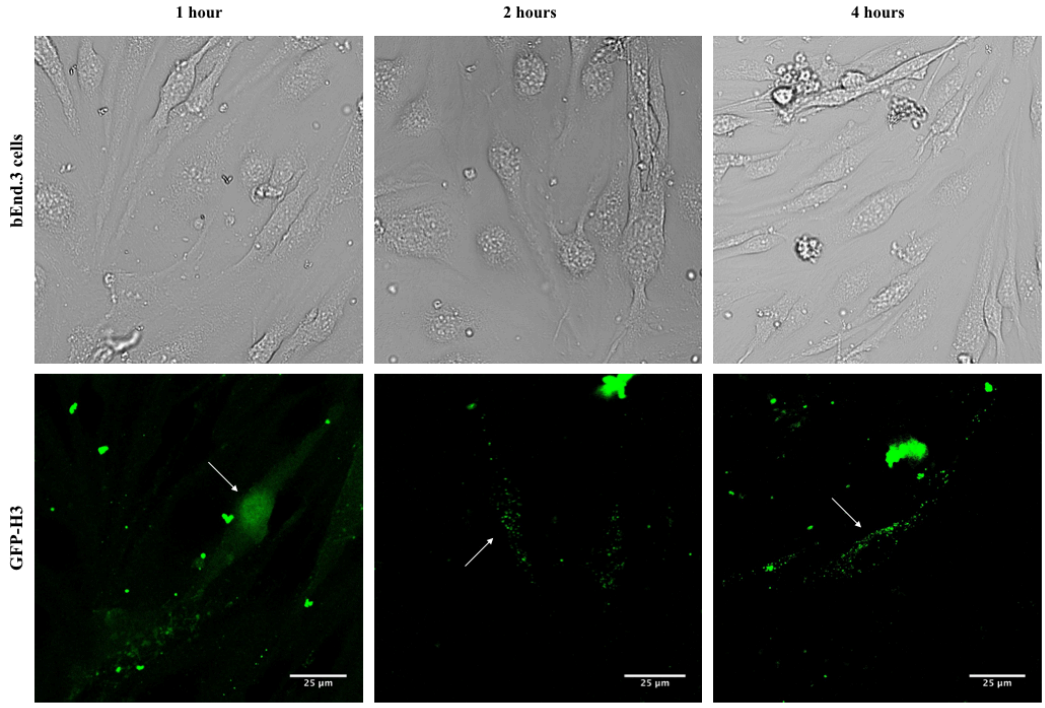

Figure III.16 - Peptide cell trafficking over time. Live bEnd.3 cells were incubated with 5 µM of GFP-H3 for 1, 2 and 4 h at 37ºC, 5 % CO_2. Images were obtained by Z-stack (7/14) with a Zeiss LSM880 microscope employing a 488 nm laser and a 20x objective. A temperature control incubator was employed at 37°C with a 5 % CO_2 supply. GFP signal is recorded in green. The scale bar represent 25 µm. The arrow points to the location of the interest cell.

The results presented in Figure III.16 show that at one-hour incubation the peptide is scattered throughout the cell. However, after a 2 and a 4 hours' incubation the protein is located in specific cellular compartments. From these results we can hypothesise that a peptide incubation of 1 hour might have concentrated the peptide in the cellular membrane. And that, over time its location is more restricted inside the cell. However, to apprehend into which cell compartment the peptide is driven it is necessary to label it with a fluorescent probe.

III.4.2. Fluorescent labelling to locate the GFP-H3 in cells

To understand the cellular compartments in which the peptide traffic and localize, organelle specific fluorescence probes were used. Since, the peptide is conjugated with GFP, RFP was

selected as the fluorescent probe for organelles in order to distinguish the labelled organelles of the labelled peptide. This allows us to obtain a yellow signal if the peptide interacts with a particular cellular compartment.

When the cells are incubated with the peptide, the first cellular structure it will encounter is the cellular membrane. Thus, to visualize cell membranes it used 5 μg/mL of CellMask™ Deep Red plasma membrane stain for 15 minutes after peptide incubation. CellMask™ is composed of amphipathic molecules that offer a lipophilic moiety for membrane loading and a negatively charged hydrophilic dye that allows its "anchoring" to the plasma membrane.

To study the peptide interaction with membrane, the cells were incubated with 5 μM at GFP-H3 during 30 minutes, 1, 2 and 3 hours. Figure III.17, shows the results obtained at these time points. At 30 minutes the peptide appears to be outside of the cells, in the medium, where some peptide aggregates are visible. However, after 1 hour, the images confirm the previously obtained, the peptide is found throughout the cell but when both fluorescence signals are merged, a co-localization was not observed which probably means the peptide is inside the cell. At 2 hours, the images reveal that peptide is inside the cells, apparently in specific compartments. Moreover, at 3 hours, we can observe the peptide inside the cell but it is also possible to observe peptide and aggregates outside the cell. Apparently, the GFP-H3 crosses the cell membrane very quickly because no co-localization signal was observed for tested time-points. However, these results suggest that the peptide can cross into the cell and exit at a later time.

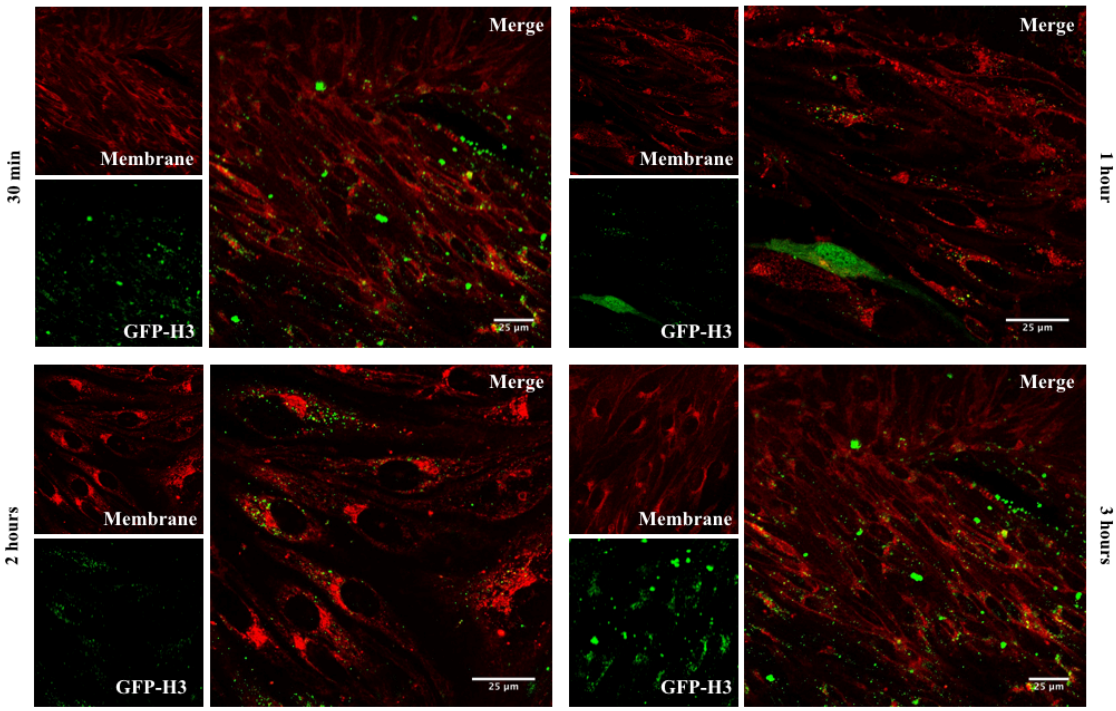

Figure III.17 - Membrane interaction experiment of PepH3. Live bEnd.3 cells were incubated with 5 µM of GFP-H3 for 30 minutes, 2 and 3 h at 37ºC, 5 % CO_2. Images were obtained with a Zeiss LSM880 microscope employing 488 and 633 nm lasers and a 63x oil objective. A temperature control incubator was employed at 37°C with a 5 % CO_2 supply. GFP signal is recorded in green while the deep red signal is recorded in red. The scale bar represent 25 µm.

As previous described, after crossing the cellular membrane the peptide might form vesicles that fuse with early endosomes that may follow different routes. Transferrin, for example, is a monomeric serum glycoprotein that binds up to two Fe^{3+} atoms. It is processed in the late endosomes, after which the transferrin receptors are recycled via a recycling endosome to the plasma membrane.[71,72] Transferrin conjugates can be used to observe transferrin trafficking in living cells and is mainly used in endocytosis investigation assays since it allows the observation various endosomes and lysosomes. So, to observe the peptide localization inside the cells, these were incubated with 5 µM of GFP-H3 for 1, 2 and 3 hours, as at these time points it was possible to observe the peptide inside the cells. Then, the cells were washed with cold PBS and incubated for 15 minutes with 25 µg/mL of transferrin from human serum Alexa Fluor® 568 conjugate.

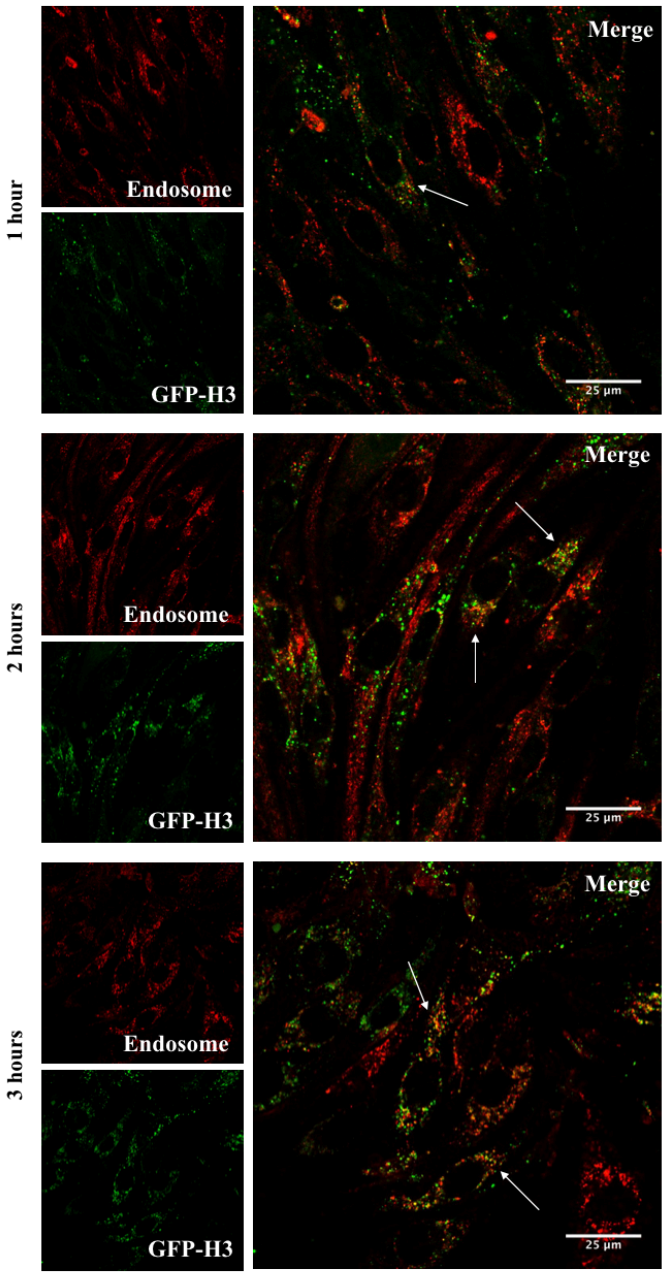

Figure III.18 - Endosomal localization experiment of PepH3. Live bEnd.3 cells were incubated with 5 µM of GFP-H3 for 1, 2 and 3 h at 37ºC, 5 % CO_2. Images were obtained with a Zeiss LSM880 microscope employing 488 and 633nm lasers and a 63x oil objective. A temperature control incubator was employed at 37°C with a 5 % CO_2 supply. GFP signal is recorded in green while the deep red signal is recorded in red. The scale bar represent 25 µm. The arrow points to the co-localization signals.

Figure III.18 shows the peptide trafficking over time. With 1-hour incubation, it is possible to observe the peptide inside the cells and when the channels are merged it is possible to observe some co-localization. However, after a 2 and a 3-hour incubation the co-localization's fluorescence signal is more intense. Probably, after a 2-hour incubation the peptide may be located in the early endosomes but after the 3-hour incubation the peptide might be in recycling

or late endosomes or in the lysosomes. The main function of these last organelles is the destruction of various biomolecules. This being the case, if the peptide is retained in the lysosomes, it will eventually be destroyed. Therefore, to test this hypothesis, the cells were labelled with a lysosome probe.

LysoTracker® Red DND-99 is an acidotropic probes that is linked to a weak base that is only partially protonated at neutral pH, and that is freely permeant to cell membranes and typically concentrates in spherical acid organelles. In these assays, the cells were incubated with 5 µM of GFP-H3 for 4 hours. After peptide incubation, the cells were incubated with 100 nM of LysoTracker® Red DND-99 for 15 minutes.

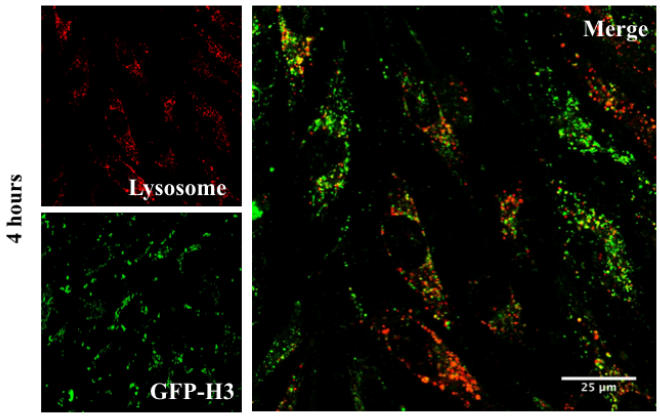

Figure III.19 - Lysosomes localization experiment of PepH3. Live bEnd.3 cells were incubated with 5 µM of GFP-H3 for 4 h at 37ºC, 5 % CO_2. Images were obtained with a Zeiss LSM880 microscope employing 488 and 561nm lasers and a 63x oil objective. A temperature control incubator was employed at 37°C with a 5% CO_2 supply. GFP signal is recorded in green while the deep red signal is recorded in red. The scale bar represent 25 µm.

The microscopy images displayed in Figure III.19 shows that a large amount of peptide is inside cells. However, co-localization of GFP with lysosomes is reduced or inexistent, revealing that the peptide escapes this degradative cellular organelle.

To complete the work presented it was intended to label other cellular compartments, such as plasma membrane, actin, early endosomes, and lysosome. However, for the labelling of these compartments is required to use a different approaches, either immunostaining using antibodies, which requires cell fixation; or using transfection of specific proteins, using CellLight® reagents. It was decided to use the last since it enable live imaging and avoids unwanted effects of cellular fixation. The CellLight® reagent, is a new fluorescent protein-signal peptide fusion that provides precise and specific targeting of cellular structures in live-cell imaging. These reagents are transfected and expressed in cells to label a specific compartment. According to the product protocol, the CellLight® reagent works better in concentrations between 10 and 50

particles per cell (PPC) and that it should be transfected when the cells show a confluence of no more than 70 % during 16 hours or more.

To test this reagent with bEnd.3 cells it was used CellLight® for lysosomes, once it could be compared with LysoTracker®. After testing different incubation times and different PPCs, the transfection was not efficient in bEnd.3 cells (data not shown). In addition, some toxic effects were observed, cell doubling time increased and cell morphology was different from healthy cells. Thus, staining of remaining compartments with this reagent was discontinued.

III.4.3. Endocytosis inhibition studies by confocal microscopy

In order to understand the endocytotic mechanism used by PepH3 to translocate the BBB and to confirm the results obtained through the BBB model, the cells were observed with a confocal microscope in the presence of endocytic inhibitors. These assays were performed in same conditions that the inhibition studies in the BBB model. The results obtained are presented in Figure III.20. The microscope parameters were adjusted from the fluorescence signal of the control sample (No drug). In this control sample the cells were incubated solely with GFP-H3, and no inhibitors were added.

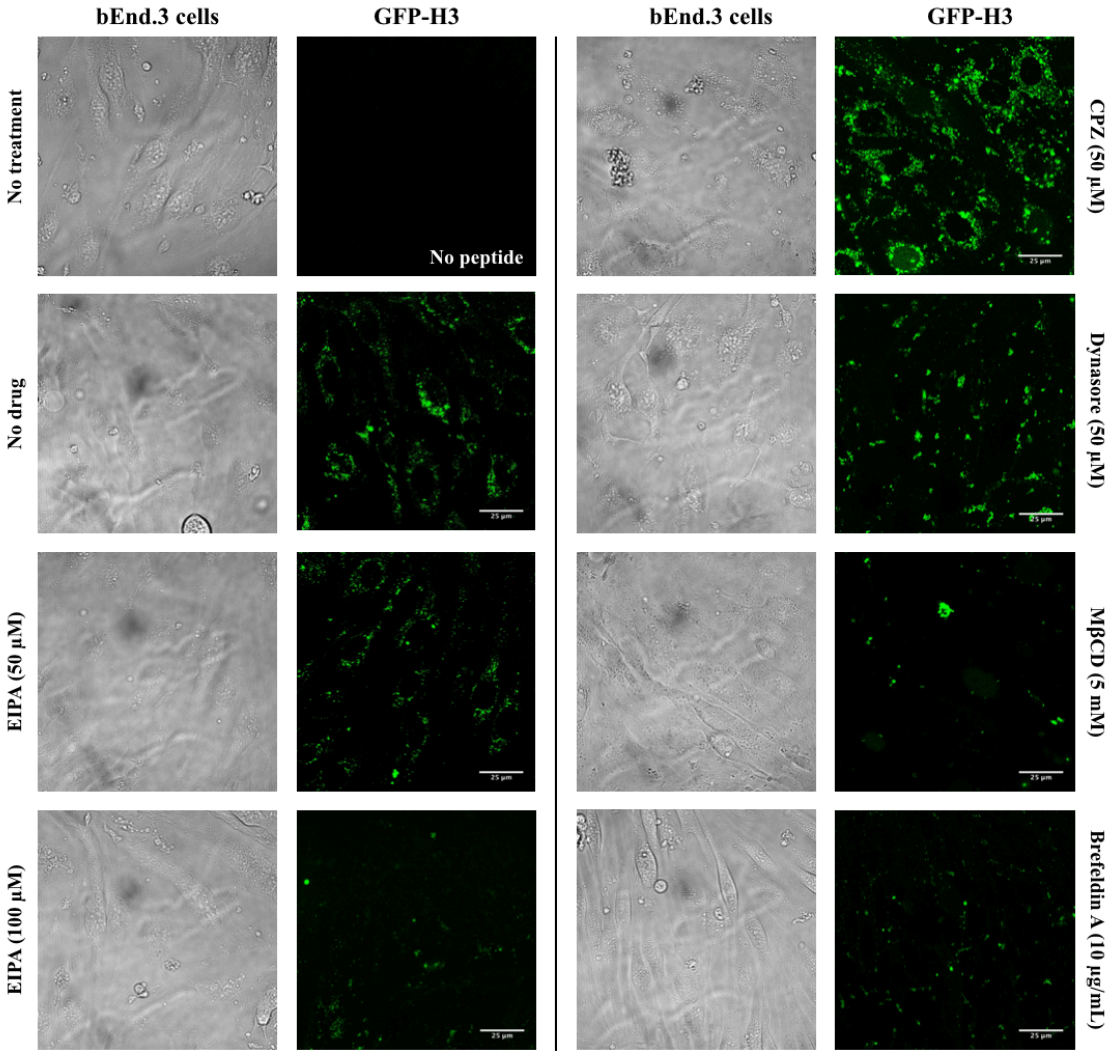

Figure III.20 - Screening of PepH3 cellular internalization routes. Live bEnd.3 cells were pre-treated with the indicated inhibitor prior to its incubation with 5 µM of GFP-H3 for 4 h at 37ºC, 5 % CO_2. Images were obtained with a Zeiss LSM880 microscope employing a 488 nm laser and a 63x oil objective. A temperature control incubator was employed at 37°C with a 5% CO_2 supply. GFP signal is recorded in green. The scale bar represent 25 µm.

In Figure III.20, the green colour shows the GFP signal emitted by GFP-H3 in different conditions. After the cells were incubated solely with GFP-H3, and no inhibitors were added (No drug sample) we can observe a good fluorescence signal into the cells.

In general, the results obtained in these assays are similar to those attained in *in vitro* studies. When the inhibitor dynasore is present, it is not possible to observe the peptide inside the cells and those found in the extracellular medium have aggregated. As for the pre-incubation of cells with CPZ it had no detectable effects in the peptide translocation. However, in contrast, the incubation of the cells with MβCD inhibits peptide translocation.

When the cells are incubated with EIPA it is possible to observe that the inhibition of peptide translocation is related to its concentration. Some inhibitors, such as EIPA, have a concentration range where they are effective. In this case, the literature suggests that EIPA is effective in the

range of 50 to 100 μM. At a concentration of 50 μM we can see that there are peptides in the cells as in the control sample, not incubated with inhibitors. In opposition, at a concentration of 100 μM, no peptide is observed in the cells.

After a pre-incubation of the cells with Brefeldin A no observable peptide is found in the cells, however it is possible to observe a fluorescence signal in extracellular media. Once the peptide is incubated after the incubation with the inhibitor, these extracellular peptides are probably, peptides that could not translocate into the cell or are peptides that may have been internalized but were removed from the cell by other pathways that do not require interaction with the Golgi apparatus.

The results obtained in *in vitro* assays, show that PepH3 internalization is sensitive to MβCD and EIPA, suggesting that PepH3 might be internalized through a lipid-raft/caveolin-mediated endocytosis or macropinocytosis. However, the internalization route is also dependent on the peptide cargo. GFP is a large cargo that may drive the peptide to be internalized via a macropinocytosis route. Moreover, dynamin was shown to have an important role in peptide internalization because no peptide was observed inside the cells but, large amount of peptide aggregates was visible in extracellular media and the image obtained in visible light shows that the cells do not exhibit their normal morphology. Probably peptides concentrated on the membrane but, the formation of endocytic vesicles could not be completed due to the inhibition of dynamin. As the concentration of peptides in the outside of the cellular membrane increases the aggregates that are visible in the image are formed. In the case of Brefeldin A, the *in vitro* results show that the membrane monolayer was perturbed but, as seen in the visible microscopy images, a normal cellular morphology is observed.

Globally, the results show that an endocytic process may be involved in the route of PepH3 internalization.

IV. CONCLUSIONS, FINAL REMARKS AND FUTURE WORK

IV. CONCLUSIONS, FINAL REMARKS AND FUTURE WORK

In recent years, cell-penetrating peptides (CPPs) have been investigated for their ability to deliver various cargoes, such as therapeutic biomolecules, across membranes and biological barriers, being potential effective vehicles in advanced treatments of CNS (central nervous system) diseases. Despite the large number of prospective applications of CPPs, the mechanism by which translocation of the blood-brain barrier (BBB) occurs remains essentially unknown. Currently, little is reported in the literature concerning the BBB translocation mechanism of these peptides and a good CPP may eventually not be a good BBB translocator. For example, in the case of PepH2 and PepH3, the latter has good translocation capacity while PepH2 heavily associates to cellular membranes and accumulates inside cells.

The main propose of the present work was to understand the mechanisms whereby PepH3, derived from the supercharged protein DEN2C, translocates the BBB.

Before exploring the translocation mechanisms, we started by conjugating the peptide with GFP. The recombinant sequences were amplified by PCR and cloned into two different expression vectors, pET28a (+) and pETM-10. We observed that, when expressed in the pETM-10 vector, the protein was retained in inclusion bodies (insoluble fraction), making its isolation more difficult. However, when the protein was expressed in pET28a (+) high levels of expression were obtained in the soluble fraction, simplifying its isolation and purification. Therefore, pET28a (+) was used to express all GFP conjugates.

In the second part of this work, the conjugates were tested in an *in vitro* BBB model, consisting of a bEnd.3 cell monolayer. In order to optimize the assay conditions, different peptide concentrations were used. Higher concentrations of peptide caused the formation of aggregates and consequent destruction of the cell monolayer. On the other hand, with a lower peptide concentration there was little peptide translocation. Therefore, the optimal concentration for *in vitro* assays was established between 0.1 μM and 1 μM. All *in vitro* assays were performed applying 0.5 μM of peptide conjugates. Another limiting factor in *in vitro* BBB assays is the buffer/medium used. It was shown that for long incubations (higher than 2 hours) the integrity of bEnd.3 cells monolayer was lost when transport buffer was used. In brief, the best conditions were obtained when the cells were incubated with 0.5 μM of GFP-H3 in complete medium for 5 hours at 37°C, 5 % CO_2, with 21.63% ± 4.81 of peptide was able to translocate the BBB.

To assess the mechanism by which novel peptide (GFP-H3) and other known CPPs (GFP-Tat and GFP-PTT) translocate the BBB, it was first tested a temperature block (4°C). By lowering temperature, the translocation of GFP-H3 decreased to 4.63% ± 0.79, suggesting that GFP-H3 cellular uptake occurs through an energy-dependent mechanism. To analyse this effect further ATP depleted environment (using sodium azide) could also be tested.[73]

The various cellular trafficking processes can be blocked using specific inhibitors. Our results reveal that the GFP-H3 requires dynamin for an efficient uptake but does not need clathrin. Additionally, both *in vitro* and confocal microscopy studies, suggest that GFP-H3 uses the lipid-raft/caveolin-mediated endocytosis because the cellular uptake is inhibited by dynasore and MβCD. Moreover, the GFP-H3 internalization is also inhibited by 100 μM of EIPA, revelling that GFP-H3 can also translocate the BBB by macropinocytosis. Together the use of temperature block and inhibitors prove that GFP-H3 uses an endocytic route for BBB translocation.

The labelling of specific cellular compartments such as cellular membrane, endosomes and lysosomes aided to clarify which compartments GFP-H3 co-localize. For the time points tested was not possible to observe co-localization with the cellular membrane. Either peptide internalization was to fast to be recorded or internalization occurs at a single molecule level, which confocal microscopy is not sensitive enough to detect. In addition, GFP-H3 is using an endocytic route in which endosomes are involved. However, GFP-H3 escapes the degradative conditions of the lysosomes, since no co-localization with this compartments was visualized (Figure III.19). Therefore, we have demonstrated the GFP-H3 is internalized via a route dependent of dynamin and lipid-rafts, in addition macropinocytosis seems to also play a role, probably by taking up protein aggregates. Following membrane internalization, GFP-H3 is sorted in early endosomes and by escaping the lysosomes appears to follow the recycling route being exocytosis. Yet, complementary studies are required to confirm the translocation mechanism.

To further elucidate the internalization mechanisms and intracellular trafficking it is important to test other inhibitors as well as new labels for specific cellular compartments. For example, we can use poly-L-lysine as membrane charge neutralizer to study the interaction of the peptide with the cellular membrane.[5]

One hypothesis to confirm the endocytosis pathways is through the study of Rho and Rac. These are two GTPases involved in cytoskeletal reorganization and endosomal trafficking. Rac is located near the plasma membrane and initiates actin polymerization at the start of macropinosome formation, while Rho is downstream of multiple endocytic pathways, including caveolin-mediated and clathrin-independent endocytosis.[49] To study the intracellular route we can label the early endosomes as well as the recycling and late endosomes by immunostaining using specific antibodies.

To confirm the qualitative microscopy results it would be important to perform a quantitative analysis to detect the amount of peptide that is within the cells and within a specific cellular compartment. Subsequently, these results would be compared to other quantitative techniques such as flow cytometry.

Subsequently, it is also important to conjugate the PepH3 with a therapeutic drug in order to verify if cargo alterations can influence the translocation mechanism and, in addition, peptide stability under physiological conditions should be tested in mouse and human serum to ensure its efficiency before *in vivo* experiments.

V. BIBLIOGRAPHY

V. BIBLIOGRAPHY

(1) Svensen, N., Walton, J. G. a, and Bradley, M. (2012) Peptides for cell-selective drug delivery. *Trends Pharmacol. Sci. 33*, 186–192.

(2) Rizzuti, M., Nizzardo, M., Zanetta, C., Ramirez, A., and Corti, S. (2015) Therapeutic applications of the cell-penetrating HIV-1 Tat peptide. *Drug Discov. Today 20*, 76–85.

(3) Reitz, C. (2012) Alzheimer's Disease and the Amyloid Cascade Hypothesis: A Critical Review. *Int. J. Alzheimers. Dis. 2012*, 1–11.

(4) Antoniou, X., and Borsello, T. (2010) Cell permeable peptides: A promising tool to deliver neuroprotective agents in the brain. *Pharmaceuticals 3*, 379–392.

(5) Gabathuler, R. (2010) Approaches to transport therapeutic drugs across the blood–brain barrier to treat brain diseases. *Neurobiol. Dis. 37*, 48–57.

(6) Muruganandam, A., Tanha, J., Narang, S., and Stanimirovic, D. (2002) Selection of phage-displayed llama single-domain antibodies that transmigrate across human blood-brain barrier endothelium. *FASEB J. 16*, 240–2.

(7) Johnson, R. M., Harrison, S. D., and Maclean, D. (2011) Therapeutic Applications of Cell-Penetrating Peptides *683*.

(8) Georgieva, J., Hoekstra, D., and Zuhorn, I. (2014) Smuggling Drugs into the Brain: An Overview of Ligands Targeting Transcytosis for Drug Delivery across the Blood–Brain Barrier. *Pharmaceutics 6*, 557–583.

(9) Banks, W. A. (2015) Peptides and the blood–brain barrier. *Peptides*.

(10) Pardridge, W. M. (2005) The blood-brain barrier: bottleneck in brain drug development. *NeuroRx 2*, 3–14.

(11) Kang, T., Gao, X., and Chen, J. (2014) Harnessing the Capacity of Cell-Penetrating Peptides for Drug Delivery to the Central Nervous System 220–230.

(12) Pardridge, W. M. (2012) Drug transport across the blood–brain barrier. *J. Cereb. Blood Flow Metab. 32*, 1959–1972.

(13) Abbott, N. J., Patabendige, A. A. K., Dolman, D. E. M., Yusof, S. R., and Begley, D. J. (2010) Structure and function of the blood–brain barrier. *Neurobiol. Dis. 37*, 13–25.

(14) Strazielle, N., and Ghersi-Egea, J. F. (2013) Physiology of blood-brain interfaces in relation to brain disposition of small compounds and macromolecules. *Mol. Pharm. 10*, 1473–1491.

(15) Cecchelli, R., Berezowski, V., Lundquist, S., Culot, M., Renftel, M., Dehouck, M.-P., and Fenart, L. (2007) Modelling of the blood–brain barrier in drug discovery and development. *Nat. Rev. Drug Discov. 6*, 650–661.

(16) Chen, Y., and Liu, L. (2012) Modern methods for delivery of drugs across the blood-brain barrier. *Adv. Drug Deliv. Rev. 64*, 640–665.

(17) Milletti, F. (2012) Cell-penetrating peptides: classes, origin, and current landscape. *Drug Discov. Today 17*, 850–860.

(18) Mo, R. H., Zaro, J. L., and Shen, W. C. (2012) Comparison of cationic and amphipathic cell penetrating peptides for siRNA delivery and efficacy. *Mol. Pharm. 9*, 299–309.

(19) Herce, H. D., and Garcia, A. E. (2007) Cell penetrating peptides: How do they do it? *J. Biol. Phys. 33*, 345–356.

(20) Stewart, K. M., Horton, K. L., and Kelley, S. O. (2008) Cell-penetrating peptides as delivery vehicles for biology and medicine. *Org. Biomol. Chem. 6*, 2242–2255.

(21) Fonseca, S. B., Pereira, M. P., and Kelley, S. O. (2009) Recent advances in the use of cell-penetrating peptides for medical and biological applications☆. *Adv. Drug Deliv. Rev. 61*, 953–964.

(22) Koren, E., and Torchilin, V. P. (2012) Cell-penetrating peptides: breaking through to the other side. *Trends Mol. Med. 18*, 385–393.

(23) Zahid, M., and Robbins, P. D. (2015) Cell-Type Specific Penetrating Peptides: Therapeutic Promises and Challenges. *Molecules 20*, 13055–70.

(24) Mäe, M., and Langel, Ü. (2006) Cell-penetrating peptides as vectors for peptide, protein and oligonucleotide delivery. *Curr. Opin. Pharmacol. 6*, 509–514.

(25) Fernández-Carneado, J., Kogan, M. J., Pujals, S., and Giralt, E. (2004) Amphipathic Peptides and Drug Delivery. *Biopolym. - Pept. Sci. Sect. 76*, 196–203.

(26) De Figueiredo, I. R., Freire, J. M., Flores, L., Veiga, A. S., and Castanho, M. a R. B. (2014) Cell-penetrating peptides: A tool for effective delivery in gene-targeted therapies. *IUBMB Life 66*, 182–194.

(27) Markoff, L., Falgout, B., and Chang, a. (1997) A conserved internal hydrophobic domain mediates the stable membrane integration of the dengue virus capsid protein. *Virology 233*, 105–117.

(28) Cruz-Oliveira, C., Freire, J. M., Conceicao, T. M., Higa, L. M., Castanho, M. A. R. B., and Da Poian, A. T. (2015) Receptors and routes of dengue virus entry into the host cells. *FEMS*

Microbiol. Rev. 39, 155–170.

(29) Ma, L., Jones, C. T., Groesch, T. D., Kuhn, R. J., and Post, C. B. (2004) Solution structure of dengue virus capsid protein reveals another fold. *Proc. Natl. Acad. Sci. 101*, 3414–3419.

(30) Freire, J. M., Veiga, A. S., Rego de Figueiredo, I., de la Torre, B. G., Santos, N. C., Andreu, D., Da Poian, A. T., and Castanho, M. a R. B. (2014) Nucleic acid delivery by cell penetrating peptides derived from dengue virus capsid protein: design and mechanism of action. *FEBS J. 281*, 191–215.

(31) Freire, J. M., Almeida Dias, S., Flores, L., Veiga, a. S., and Castanho, M. a. R. B. (2015) Mining viral proteins for antimicrobial and cell-penetrating drug delivery peptides. *Bioinformatics 8*, 1–5.

(32) Freire, J. M., Veiga, A. S., de la Torre, B. G., Santos, N. C., Andreu, D., Da Poian, A. T., and Castanho, M. a R. B. (2013) Peptides as models for the structure and function of viral capsid proteins: Insights on dengue virus capsid. *Biopolymers 100*, 325–36.

(33) Freire, J. M., Santos, N. C., Veiga, A. S., Da Poian, A. T., and Castanho, M. A. R. B. (2015) Rethinking the capsid proteins of enveloped viruses: Multifunctionality from genome packaging to genome transfection. *FEBS J. 282*, 2267–2278.

(34) Freire, J. M., Veiga, A. S., Conceição, T. M., Kowalczyk, W., Mohana-Borges, R., Andreu, D., Santos, N. C., Da Poian, A. T., and Castanho, M. A. R. B. (2013) Intracellular nucleic acid delivery by the supercharged dengue virus capsid protein. *PLoS One 8*.

(35) Neves, V., Aires-da-Silva, F., Morais, M., Gano, L., Pinto, A., Aguiar, S., Gaspar, D., Fernandes, C., Correia, J. D. G., and Castanho, M. Novel peptides derived from Dengue virus capsid protein translocate reversibly the blood-brain barrier through a receptor-free mechanism. *Submited to ACS Chem. Biol.*

(36) Deshayes, S., Morris, M. C., Divita, G., and Heitz, F. (2005) Cell-penetrating peptides: tools for intracellular delivery of therapeutics. *Cell. Mol. Life Sci. 62*, 1839–1849.

(37) Di Pisa, M., Chassaing, G., and Swiecicki, J.-M. (2015) Translocation Mechanism(s) of Cell-Penetrating Peptides: Biophysical Studies Using Artificial Membrane Bilayers. *Biochemistry 54*, 194–207.

(38) Lalatsa, A., Schatzlein, A. G., and Uchegbu, I. F. (2014) Strategies to deliver peptide drugs to the brain. *Mol. Pharm. 11*, 1081–93.

(39) McCrudden, M. T. C., Singh, T. R. R., Migalska, K., and Donnelly, R. F. (2013) Strategies for enhanced peptide and protein delivery. *Ther. Deliv. 4*, 593–614.

(40) Hervé, F., Ghinea, N., and Scherrmann, J.-M. (2008) CNS Delivery Via Adsorptive

Transcytosis. *AAPS J. 10*, 455–472.

(41) De Bock, M., Van Haver, V., Vandenbroucke, R. E., Decrock, E., Wang, N., and Leybaert, L. (2016) Into rather unexplored terrain-transcellular transport across the blood-brain barrier. *Glia* n/a-n/a.

(42) Duchardt, F., Fotin-Mleczek, M., Schwarz, H., Fischer, R., and Brock, R. (2007) A comprehensive model for the cellular uptake of cationic cell-penetrating peptides. *Traffic 8*, 848–866.

(43) Foerg, C., and Merkle, H. P. (2007) On The Biomedical Promise of Cell Penetrating Peptides: Limits Versus Prospects. *J. Pharm. Sci. 99*, 4215–4227.

(44) Takei, K., and Haucke, V. (2001) Clathrin-mediated endocytosis: Membrane factors pull the trigger. *Trends Cell Biol. 11*, 385–391.

(45) Foged, C., and Nielsen, H. M. (2008) Cell-penetrating peptides for drug delivery across membrane barriers 105–118.

(46) Heitz, F., Morris, M. C., and Divita, G. (2009) Twenty years of cell-penetrating peptides : from molecular mechanisms to therapeutics. *Br. J. Pharmacol.* 195–206.

(47) Zorko, M., and Langel, U. (2005) Cell-penetrating peptides: mechanism and kinetics of cargo delivery. *Adv. Drug Deliv. Rev. 57*, 529–545.

(48) Singapore, N. U. of. MBInfo. *2016*. Retrieved August 2016, from www.mechanobio.info.

(49) Thompson, D. B., Villaseñor, R., Dorr, B. M., Zerial, M., and Liu, D. R. (2012) Cellular uptake mechanisms and endosomal trafficking of supercharged proteins. *Chem. Biol. 19*, 831–843.

(50) Cecchelli, R., Dehouck, B., Descamps, L., Fenart, L., Buée-Scherrer, V., Duhem, C., Lundquist, S., Rentfel, M., Torpier, G., and Dehouck, M. P. (1999) In vitro model for evaluating drug transport across the blood-brain barrier. *Adv. Drug Deliv. Rev. 36*, 165–178.

(51) Watson, P., Jones, A. T., and Stephens, D. J. (2005) Intracellular trafficking pathways and drug delivery: Fluorescence imaging of living and fixed cells. *Adv. Drug Deliv. Rev. 57*, 43–61.

(52) Zou, L.-L., Ma, J.-L., Wang, T., Yang, T.-B., and Liu, C.-B. (2013) Cell-penetrating Peptide-mediated therapeutic molecule delivery into the central nervous system. *Curr. Neuropharmacol. 11*, 197–208.

(53) Shehu Mustapha, I. (2006) Quantitative Fluorescence Microscopy of Protein Dynamics in Living Cells. *Science (80-.).*

(54) Pawley, J. B. (2006) Handbook of Biological Confocal Microscopy (Pawley, J. B., Ed.)

Thrird edi. Springer.

(55) Davidson, M. W., University, F. S., Florida, U. of, and Laboratory, L. A. N. (1995) Molecular Expressions.

(56) Davidson, M. W., and Day, R. N. Zeiss. Retrieved August 2016, from http://zeiss-campus.magnet.fsu.edu/articles/probes/jellyfishfps.html

(57) Davidson, M. W. MicroscopyU. *Nikon Instruments Inc.*Retrieved August 2016, from www.microscopyu.com.

(58) Amos, W. B., and White, J. G. (2003) How the confocal laser scanning microscope entered biological research. *Biol. Cell 95*, 335–342.

(59) Microsystems, L. Science Lab. *Leica Microsystems*. Retrieved August 2016, from www.leica-microsystems.com/science-lab/.

(60) Smith, C. L. (2011) Basic confocal microscopy. *Curr. Protoc. Neurosci.* 1–18.

(61) Paddock, S. W. (2000) Principles and practices of laser scanning confocal microscopy. *Mol. Biotechnol. 16*, 127–149.

(62) Inc., O. A. (2012) Microscopy Resource Center. *Olympus Am. Inc.* Retrieved August 2016, from http://olympus.magnet.fsu.edu/index.html.

(63) Stephens, D. J., and Allan, V. J. (2003) Light Microscopy Techniques for Live Cell Imaging. *Biol. Imaging 82*, 82–86.

(64) Dümmler, A., Lawrence, A.-M., and de Marco, A. (2005) Simplified screening for the detection of soluble fusion constructs expressed in E. coli using a modular set of vectors. *Microb. Cell Fact. 4*, 34.

(65) Cronican, J. J., Thompson, D. B., Beier, K. T., McNaughton, B. R., Cepko, C. L., and Liu, D. R. (2010) Potent delivery of functional proteins into Mammalian cells in vitro and in vivo using a superchCronican, J. J., Thompson, D. B., Beier, K. T., McNaughton, B. R., Cepko, C. L., & Liu, D. R. (2010). Potent delivery of functional proteins into Mammalian cel. *ACS Chem. Biol. 5*, 747–52.

(66) Vercauteren, D., Vandenbroucke, R. E., Jones, A. T., Rejman, J., Demeester, J., De Smedt, S. C., Sanders, N. N., and Braeckmans, K. (2010) The use of inhibitors to study endocytic pathways of gene carriers: optimization and pitfalls. *Mol. Ther. 18*, 561–569.

(67) Ivanov, A. (2008) Pharmacological Inhibition of Endocytotic Pathways: Is It Specific Enough to Be Useful? *Exocytosis Endocytosis – Methods Mol. Biol. 440*, 15–33.

(68) Macia, E., Ehrlich, M., Massol, R., Boucrot, E., Brunner, C., and Kirchhausen, T. (2006)

Dynasore, a Cell-Permeable Inhibitor of Dynamin. *Dev. Cell 10*, 839–850.

(69) Ferguson, S. M., and Camilli, P. De. (2012) Dynamin, a membrane-remodelling GTPase. *Nat. Publ. Gr. 13*, 75–88.

(70) Fittipaldi, A., Ferrari, A., Zoppé, M., Arcangeli, C., Pellegrini, V., Beltram, F., and Giacca, M. (2003) Cell Membrane Lipid Rafts Mediate Caveolar Endocytosis of HIV-1 Tat Fusion Proteins. *J. Biol. Chem. 278*, 34141–34149.

(71) Neves, V., Gerondopoulos, A., Heister, E., Tîlmaciu, C., Flahaut, E., Soula, B., Silva, S. R. P., McFadden, J., and Coley, H. M. (2012) Cellular localization, accumulation and trafficking of double-walled carbon nanotubes in human prostate cancer cells. *Nano Res. 5*, 223–234.

(72) Excitation, A. F. (2007) Transferrin Conjugates 1–3.

(73) Drin, G., Cottin, S., Blanc, E., Rees, A. R., and Temsamani, J. (2003) Studies on the Internalization Mechanism of Cationic Cell-penetrating Peptides. *J. Biol. Chem. 278*, 31192–31201.

VI. APPENDIXES

VI. APPENDIXES

VI.1. Protein Sequences

GFP

MGVSKGEELFTGVVPILVELDGDVNGHKFSVSGEGEGDATYGKLTLKFICTTGKLPVP
WPTLVTTLTYGVQCFARYPDHMKQHDFFKSAMPEGYVQERTIFFKDDGNYKTRAEVK
FEGDTLVNRIELKGIDFKEDGNILGHKLEYNYNSHKVYITADKQKNGIKVNFKTRHNIE
DGSVQLADHYQQNTPIGDGPVLLPDNHYLSTQSALSKDPNEKRDHMVLLEFVTAAGIT
LGMDELYK

Molecular weight: 26954.4 Da

Ext. Coefficient: 21890 M^{-1} cm^{-1}

GFP-TAT

MGVSKGEELFTGVVPILVELDGDVNGHKFSVSGEGEGDATYGKLTLKFICTTGKLPVP
WPTLVTTLTYGVQCFARYPDHMKQHDFFKSAMPEGYVQERTIFFKDDGNYKTRAEVK
FEGDTLVNRIELKGIDFKEDGNILGHKLEYNYNSHKVYITADKQKNGIKVNFKTRHNIE
DGSVQLADHYQQNTPIGDGPVLLPDNHYLSTQSALSKDPNEKRDHMVLLEFVTAAGIT
LGMDELYKSGGGGS**GRKKRRQRRRPPQ**

Molecular weight: 30208.9 Da

Ext. Coefficient: 21890 M^{-1} cm^{-1}

GFP-PTT

MGVSKGEELFTGVVPILVELDGDVNGHKFSVSGEGEGDATYGKLTLKFICTTGKLPVP
WPTLVTTLTYGVQCFARYPDHMKQHDFFKSAMPEGYVQERTIFFKDDGNYKTRAEVK
FEGDTLVNRIELKGIDFKEDGNILGHKLEYNYNSHKVYITADKQKNGIKVNFKTRHNIE
DGSVQLADHYQQNTPIGDGPVLLPDNHYLSTQSALSKDPNEKRDHMVLLEFVTAAGIT
LGMDELYKSGGGGS**RQIKIWFQNRRMKWKK**

Molecular weight: 30966.8 Da

Ext. Coefficient: 32890 M^{-1} cm^{-1}

GFP-H3

MGVSKGEELFTGVVPILVELDGDVNGHKFSVSGEGEGDATYGKLTLKFICTTGKLPVP
WPTLVTTLTYGVQCFARYPDHMKQHDFFKSAMPEGYVQERTIFFKDDGNYKTRAEVK
FEGDTLVNRIELKGIDFKEDGNILGHKLEYNYNSHKVYITADKQKNGIKVNFKTRHNIE
DGSVQLADHYQQNTPIGDGPVLLPDNHYLSTQSALSKDPNEKRDHMVLLEFVTAAGIT
LGMDELYKSGGGGSGGGGSS**AGILKRW**

Molecular weight: 29735.3 Da

Ext. Coefficient: 27390 M^{-1} cm^{-1}

VI.2. Map of vector pET28a (+)

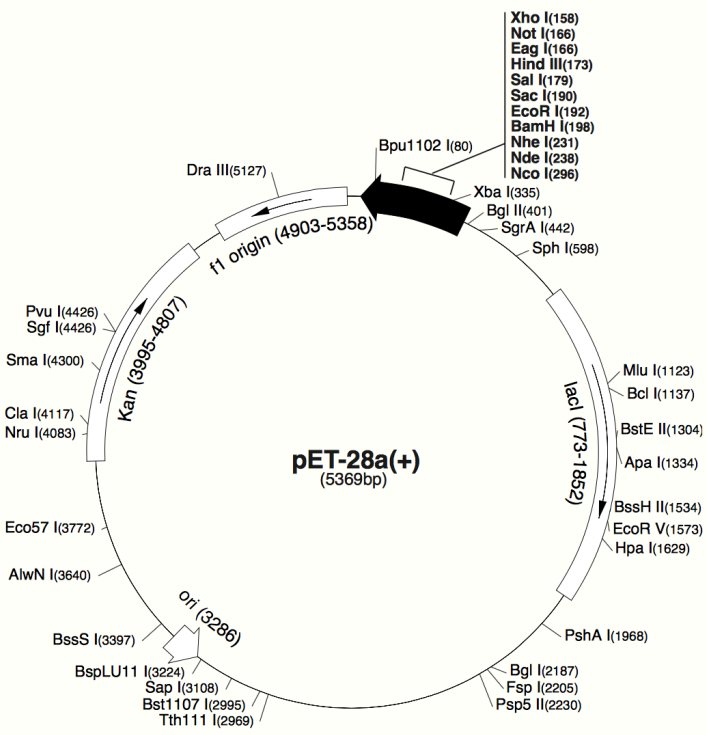

Figure VI.1 - Map of expression vector pET28a (+), Novagen.

VI.3. Map of vector pETM-10

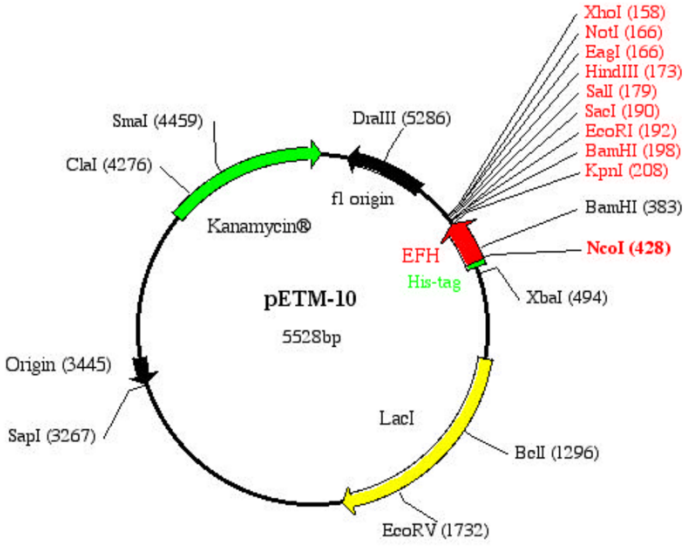

Figure VI.2 - Map of expression vector pETM-10, EMBL Protein Expression and Purification Facility.

VI.4. Growth media

Table VI.1 - Composition of all growth media used in this work.

	SB	SOB	LB	LB agar
Tryptone	24 g	16 g	8 g	-
Yeast extract	16 g	4 g	4 g	-
NaCl	-	0.4 g	8 g	-
MOPS	8 g	-	-	-
1M KCl	-	2 mL	-	-
1M $MgCl_2$	-	8 mL	-	-
LB agar	-	-	-	28 g
Final Volume of dH_2O	**800 mL**	**800 mL**	**800 mL**	**800 mL**

The pH of the LB agar solution was measured with a GLP 21 pH Meter (Crison), and adjusted to pH 7 with NaOH. All solutions were autoclaved. After sterilization, the antibiotic Kanamycin was added (50 μg/mL).

VI.5. Cell soluble extract preparation and purification flowchart

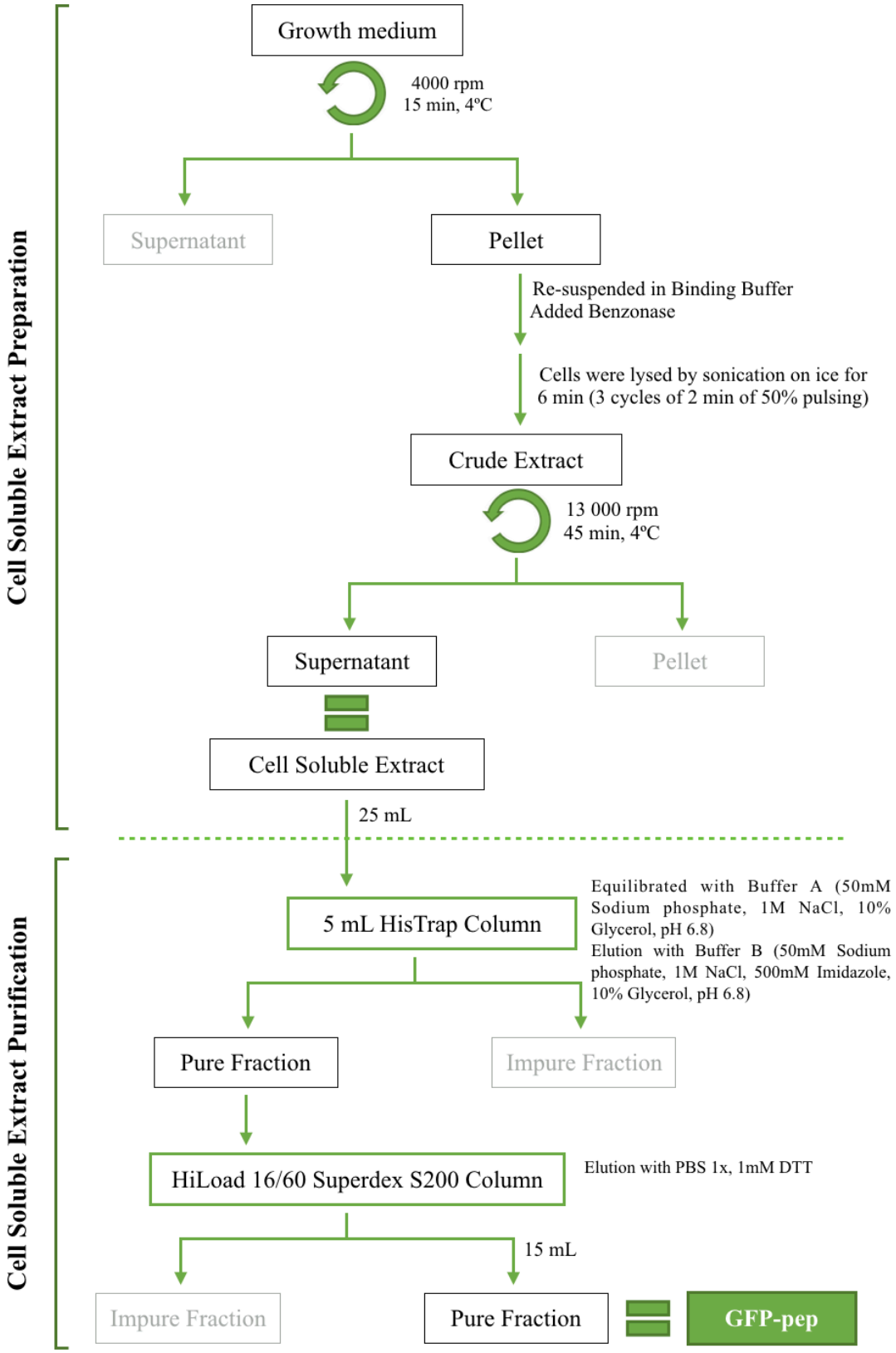

Figure VI.3 - Cell soluble extract preparation and purification flowchart.

VI.6. Protein Quantification by Bradford Method

The Bradford method is a simple and precise colorimetric assay to determine the protein concentration. This method was used to confirm the protein quantification done by NanoDrop. Sample preparation followed the manufacture's indications (Bio-Rad).

In order to use the correct concentration of BSA (0.1 mg/mL), the absorbance of the solution was measured at 279 nm. The theoretical and corrected concentration of BSA as well as the respective absorbance at 595 nm for calibration curve as showed in Table VI.2.

The protein concentration was determined applying the resulting equation from the calibration curve (Figure VI.4).

Table VI.2 - Protein concentration and absorbance values used for BSA calibration curve. MW:66400 Da; ε:43824 M^{-1} cm^{-1}

[BSA] (µg/mL)	[BSA]corrected (mg/mL)	Abs_{595nm}
8	0.0072	0.223
12	0.0108	0.328
20	0.0180	0.515
40	0.0360	0.903

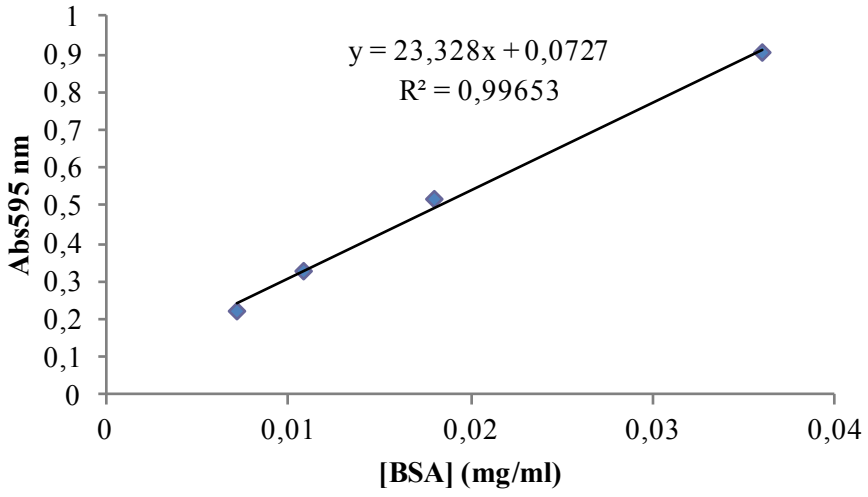

Figure VI.4 - BSA calibration curve used for protein quantification by Bradford method. Absorbance measured at 595 nm. Equation: y=23.328x + 0.0727; R^2=0.99653.

VI.7. Gel Electrophoresis

Polyacrylamide gel electrophoresis was performed in denaturant conditions SDS-PAGE to analyse the purified proteins. The gels were prepared as showed in Table VI.3 with 12% (w/v) polyacrylamide.

Table VI.3 - Preparation of a 12% polyacrylamide gel.

	Stacking gel (4%)	**Resolving gel (12%)**
30% Acrylamide/bis	1.98 mL	6 mL
0.5 M Tris-HCl, pH 6.8	3.78 mL	-
1.5 M Tris-HCl, pH 8.8	-	3.75 mL
10% SDS	150 µL	150 µL
dH_2O	9 mL	5.03 mL
TEMED	15 µL	7.5 µL
10% APS	75 µL	75 µL
Total volume	**15 mL**	**15 mL**

All samples were prepared with the addition of 20 µL of loading buffer to 3 µg/mL of sample. Samples were incubated at 100°C for 10 min. After incubation, samples were loaded into a gel and placed in 1x running buffer. Initially samples were run at 140 V, when in the stacking gel portion, and then the voltage was increased to 180 V during resolving gel portion.

Table VI.4 – Composition of loading buffer solution.

Laemmli buffer	
4% SDS	0.4 g
10% β-Mercaptoethanol	1 mL
20% Glycerol	2 mL
0.004% bromophenol blue	1.6 mL
125 mM Tris-HCl, pH 6.8	5.4 mL
Total volume	**10 mL**

Table VI.5 – Tris-Glycine buffer composition.

Running Buffer 10x	Prepared
Tris	25 mM
Glycine	190 mM
SDS	0.1%

Running buffer 10x was diluted to 1x with H_2O.

Electrophoresis gels were prepared with a Mini-Protean Tetra Cell System (Bio-Rad) using 8.3 x 7.3 cm handcast gels. The molecular weight marker used for SDS-PAGE was PageRuler Prestained Protein Ladder (Fermentas), consisting in a mixture of ten native proteins (10 to 180 kDa). An electrophoresis profile of the marker is despite in Figure VI.5.

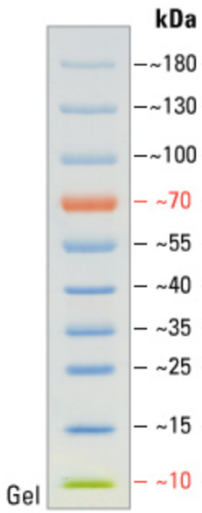

Figure VI.5 - Electrophoretic profile of Fermentas PageRuler prestained protein ladder in a 4-20% Tris-glycine gel (SDS-PAGE).

After running, gels were stained by immersion on a Coomassie Brilliant Blue staining solution and the excess dye was removed by immersion on a distaining solution. The composition of each of these solutions is presented below.

Table VI.6 – Composition of Coomassie blue dye solution.

Coomassie Brilliant Blue – Staining Solution	
Coomassie Brilliant Blue	0.5 g
50% Methanol (v/v)	250 mL
10% Glacial Acetic Acid (v/v)	50 mL
40% H_2O	200 mL
Total volume	**500 mL**

Table VI.7 – Composition of Distaining solution.

Distaining Solution	
40% Methanol (v/v)	200 mL
10% Glacial Acetic Acid (v/v)	50 mL
50% H_2O	250 mL
Total volume	**500 mL**

VI.8. Preparation of Solutions

Table VI.8 – Composition of PBS solution.

PBS	
137 mM NaCl	8 g
2.7 mM KCl	0.2 g
10 mM Na_2HPO_4	1.44 g
1.8 mM KH_2PO_4	0.24 g
Final volume with H_2O	**1 L**

Adjust the solution pH to 7.4 and sterilized by autoclave.

Table VI.9 – Composition of RIPA buffer.

RIPA Buffer	
50 mM Tris-HCl	0.788 g
150 mM NaCl	0.8766 g
1% Triton X-100	1 mL
Final volume with H_2O	**100 mL**

Adjust the solution pH to 7.2 and sterilized by autoclave.

Table VI.10 – Composition of Acid buffer.

Acid Buffer	
10 mM NaCl	0.5844 g
50 mM Glycine	0.375 g
Final volume with H_2O	**100 mL**

Adjust the solution pH to 2.8 and sterilized by autoclave.

VI.9. Gene Ladder

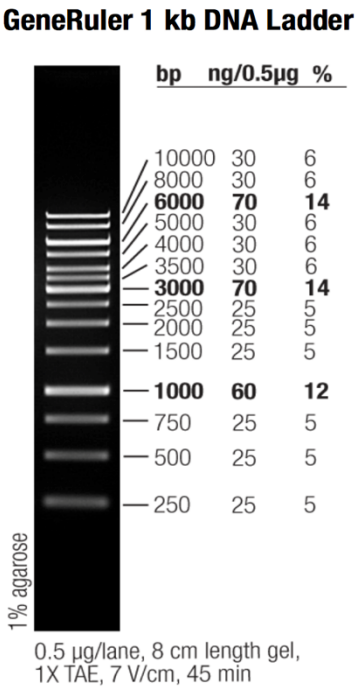

Figure VI.6 - Electrophoretic profile of Fermentas GeneRuler 1 kb DNA ladder in a 1% (w/v) agarose gel in 1x TAE buffer.

VI.10. Reagent List

Table VI.11 – Brand and purity of the reagents used in this work.

Reagent	Purity	Brand
30% Acrylamide/bis	-	Bio-Rad
Agarose Molecular Biology grade in range of 50bp-50kb	-	GeneOn
Agarose Ultrapure grade	-	Nzytech
Ammonium Persulfate (APS)	-	Bio-Rad
Anti-proteases cocktail-EDTA free	-	Roche
Benzonase® Nuclease 25 U/µL	>90%	Merck
Brefeldin A	≥99%	Sigma-Aldrich
Bromophenol Blue	-	Bio-Rad
BSA	≥98%	Merck
Cell Mask Deep Red	-	Thermo Fisher Scientific
Chlorpromazine hydrochloride	≥98%	Sigma-Aldrich
Coomassie Brilliant Blue	-	Bio-Rad
Dimethyl sulfoxide (DMSO)	≥99.8%	Merck
Dithiothreitol (DTT)	≥98%	Sigma-Aldrich
DNA Orange Loading Dye	-	Fermentas
Dulbecco's Modified Eagle's Medium (DMEM)	-	Gibco – Thermo Fisher Scientific
Dulbecco's Modified Eagle's Medium (DMEM), no phenol red	-	Gibco – Thermo Fisher Scientific
Dynasore hydrate	-	Sigma-Aldrich
Ethanol	99.85%	Merck
FD40	-	Sigma-Aldrich
Fetal Bovine Serum	-	Gibco – Thermo Fisher Scientific
Fibronectin Bovine Plasma	-	Calbiochem
Glacial Acetic acid	99.80%	Merck
Glucose	≥99.5%	Sigma-Aldrich
Glycerol anhydrous Molecular Biology Grade	99.50%	AppliChem
Glycine	≥99%	Sigma-Aldrich
Glycogen	-	Roche
Green safe	-	Nzytech
Imidazol	≥99%	Merck
Isopropanol	≥99.8%	Merck
Isopropyl β-D-1-thiogalactopyranoside (IPTG)	≥99%	Sigma-Aldrich
Kanamicin Sulphate	-	Merck
LB agar	-	AppliChem

LysoTracker Red DND-99	-	Thermo Fisher Scientific
Magnesium Chloride	-	Merck
Methanol	99.80%	Merck
Methyl-β-cyclodextrin	-	Sigma-Aldrich
MOPS	-	Merck
O'Gene Ruler Ladder 1kB	-	Fermentas
PCR Master Mix – Supreme NZyTaq 2x green	-	nzytech
Penicillin-Streptomycin (Pen Strep)	-	Gibco – Thermo Fisher Scientific
Poly-L-Lysine	-	Sigma-Aldrich
Potassium chloride	-	Merck
Potassium dihydrogen phosphate	99.5%	Merck
Protein Ladder	-	Thermo Fisher Scientific
Running buffer: Tris/Glycine/SDS	-	Bio-Rad
Sodium Acetate	≥99%	Sigma-Aldrich
Sodium chloride	-	Merck
Sodium dihydrogen phosphate monohydrate	99%	Merck
Sodium dodecyl sulphate (SDS)	≥99%	Merck
Sodium phosphate	96%	Sigma.Aldrich
TAE 50x	-	Nzytech
TBE 10x	-	Nzytech
TEMED	≥99%	Merck
Tris-HCl	-	Merck
Triton X-100	-	Merck
Trypsin	-	Gibco – Thermo Fisher Scientific
Tryptone USP	-	Biokar Diagnostics
Yeast Extract	-	Biokar Diagnostics
β-Mercaptoethanol	≥99%	Merck